9. DIFFRACTION EFFECTS IN RADIOMETRY*

Eric L. Shirley
National Institute of Standards and Technology, Gaithersburg, Maryland, USA

9.1 Introduction and Definitions

9.1.1 The Context of Traditional Radiometry

Radiometry is the measurement of energy in the form of electromagnetic radiation (i.e., light). We can specify such a measurement further by geometrical definitions that delineate the radiation that is measured. Two "end-point" delineations are self-evident in the definitions of radiance and irradiance. Radiance (denoted by L) is defined as the power that is emitted per projected unit area of source per steradian. Irradiance (denoted by E) is defined as the power incident per unit area of a surface. Radiance, irradiance and other quantities are further discussed in Chapter 1. The definitions of radiance and irradiance illustrate how traditional radiometry frequently involves transfer of electromagnetic energy from points on one surface to points on a different surface.

9.1.2 Throughput of an Optical Setup

For a given optical setup, it is standard to relate source radiance (L) to power reaching the detector (Φ) by a measurement equation [1]. In this chapter, the measurement equation can have the form

$$\Phi_\lambda(\lambda) = T(\lambda)L_\lambda(\lambda) \tag{9.1}$$

A spectral quantity such as $\Phi_\lambda(\lambda)$ is the power per unit wavelength at wavelength λ, according to the pattern,

$$\Phi = \int_0^\infty \mathrm{d}\lambda\, \Phi_\lambda(\lambda) \tag{9.2}$$

The quantity $T(\lambda)$ is the "throughput" of the optical setup under consideration. As a starting approximation, we can compute $T(\lambda)$ using ray-tracing according to geometrical optics. We then have $T(\lambda) = T_0 M(\lambda)$, where T_0 is the "geometrical throughput" of an optical setup, a purely geometrical entity, with no spectral dependence, and $M(\lambda)$, which has an

*Contribution of the National Institute of Standards and Technology.

EXPERIMENTAL METHODS IN THE PHYSICAL SCIENCES, vol. 41
ISSN 1079-4042 DOI: 10.1016/S1079-4042(05)41009-7
Published by Elsevier Inc.

ideal value of unity, can be introduced to account for optical filters, lens transmittance, mirror reflectance, and so forth. For simple setups, it is often possible to express T_0 in closed form (see Chapter 1 for an example).

9.1.2.1 Diffraction effects

Because electromagnetic radiation actually propagates as a wave entity instead of according to geometrical (ray) optics, we generally have $T(\lambda) \neq T_0 M(\lambda)$. The relationship between $T(\lambda)$ and T_0 can instead be given in the form

$$T(\lambda) = F(\lambda) T_0 M(\lambda) = [1 + \varepsilon_{\mathrm{diff}}(\lambda)] T_0 M(\lambda) \tag{9.3}$$

The quantity $F(\lambda)$ is a ratio that would be unity in the ideal case of geometrical optics. The quantity $\varepsilon_{\mathrm{diff}}(\lambda)$ is the difference between $F(\lambda)$ and unity. This difference and its impact on radiometric measurements shall be referred to as "diffraction effects" on spectral throughput or spectral power. We can also consider diffraction effects on spectral and total irradiance, point-to-point propagation of radiation, and other quantities.

Accounting for the difference between $F(\lambda)$ and unity, and its impact on measurement results shall be referred to as including "diffraction corrections." From Eq. (9.3), we may deduce that many quantities, including detector responsivity, source radiance, and geometrical throughput (as influenced, say, by the area of an aperture under test), can be inferred from a radiometric measurement. This requires sufficient knowledge of all other quantities affecting the measurement. In general, diffraction is one factor that affects the outcome. Hence, diffraction effects may need to be taken into account.

In the case of complex radiation, such as is encountered when measuring the radiance of a laboratory blackbody source, diffraction effects on the spectrally integrated signal are more relevant than diffraction effects at just one wavelength. Suppose that the output signal S of a sensor (for instance, this signal may be an output voltage) is given by $S = \int_0^\infty \mathrm{d}\lambda \, R(\lambda)\Phi_\lambda(\lambda)$, which involves a linear combination of the spectral power $\Phi_\lambda(\lambda)$ reaching the detector at each wavelength weighted by the sensor's relative spectral response, $R(\lambda)$. The diffraction effects on the signal become

$$\langle F \rangle = 1 + \langle \varepsilon_{\mathrm{diff}} \rangle = 1 + \frac{\int_0^\infty \mathrm{d}\lambda [F(\lambda) - 1] R(\lambda)\Phi_\lambda(\lambda)}{\int_0^\infty \mathrm{d}\lambda \, R(\lambda)\Phi_\lambda(\lambda)} \tag{9.4}$$

9.1.3 Chapter Organization

In what follows, aspects of diffraction effects are further discussed within the context of radiometry. Diffraction theory is first discussed, with concepts and conceptual pictures of diffraction as it affects radiometry being laid out. Only the very core essentials are discussed, with much detail left to the references.

A simplified model for diffraction effects is derived that is appropriate for describing Fresnel and Fraunhofer diffraction in systems that can be treated using Gaussian optics [2, 3]. The model is applicable to diffraction by single apertures and lenses as well as by several optical elements in series, which can often be more relevant to practical radiometry.

Nonetheless, the main diffraction effects often result from that by one optical element, which is frequently a circular aperture or lens that is placed between a coaxial circular "effective" source and "effective" detector. For example, a defining aperture that is in front of the opening of a blackbody cavity might be treatable as a Lambertian source for purposes of diffraction effects that occur downstream from the defining aperture. Therefore, diffraction effects on the cylindrically symmetrical source–aperture–detector (SAD) problem are discussed in more detail.

The radiometry literature attests to the considerable attention paid to diffraction effects. Some of this work, much of it recent, is mentioned. The role of diffraction in radiometry is still a dynamic and rapidly evolving field. Because diffraction effects are especially important at longer wavelengths, the extension of radiometry into the infrared has driven much of the need for improvement, coupled with the need for ever higher accuracy, thanks to the innovations in cryogenic radiometry. The reader should therefore also search the literature written after this volume.

Finally, brief mention is made of novel and/or unconventional radiation sources, such as synchrotrons. For these sources, novel coherence that is not present in incoherent sources such as blackbodies may require reassessing the applicability of conventional ways of thinking about diffraction effects.

9.2 Theories of Diffraction

Here, a "theory of diffraction" could operationally involve electromagnetic wave propagation in the complex geometry of an optical setup. However, we do not really want a complete description of such propagation. For purposes of diffraction studies, we want to estimate how the actual propagation differs from that predicted by geometrical optics, and how these differences affect measurements. Distilling just this information is the goal of diffraction analysis.

A complete description of the propagation of electromagnetic radiation would not only require solving Maxwell's equations that govern the radiation within free space and other media [4]. We would also need to describe the coupled motion of induced dielectric polarization and electrical currents within optical elements. Even now, this task has been carried out, for instance, in the fields of photonic band structure and optical nanostructures, only for simple or highly simplified systems [5]. Some simplifications are usually required to describe electromagnetic wave propagation in conventional optical systems.

9.2.1 Motivation of the Scalar Helmholtz Equation

Within a region of free space or some other uniform medium, the electric field $\mathbf{E}(\mathbf{x}, t)$ has the general form,

$$\mathbf{E}(\mathbf{x}, t) = \int_{-\infty}^{\infty} \mathrm{d}\omega \int_S \mathrm{d}^2\hat{\mathbf{q}} \sum_{\mu} X_{\mu}(\hat{\mathbf{q}}, \omega)\hat{\mathbf{e}}_{\mu}(\hat{\mathbf{q}}, \omega) \exp\{\mathrm{i}\omega[n_{\mu}(\hat{\mathbf{q}}, \omega)\hat{\mathbf{q}} \cdot \mathbf{x}/c - t]\} \quad (9.5)$$

Here $\mathbf{x}$ and t are space and time coordinates, ω the angular frequency, S the unit sphere, $\hat{\mathbf{q}}$ a directional unit vector, $\hat{\mathbf{e}}_{\mu}(\hat{\mathbf{q}}, \omega)$ a polarization vector for polarization μ, $n_{\mu}(\hat{\mathbf{q}}, \omega)$ an index of refraction, and c the speed of light in vacuum. Furthermore, i denotes the square root of -1, and we use the convention of time evolution having the form, $\exp(-\mathrm{i}\omega t)$. A parameter $X_{\mu}(\hat{\mathbf{q}}, \omega)$ is the complex amplitude for a particular combination of frequency, polarization and direction of propagation. The magnetic induction $\mathbf{B}(\mathbf{x}, t)$ may be found from $\mathbf{E}(\mathbf{x}, t)$ using Maxwell's equations, which formally completes one aspect of describing electromagnetic wave propagation.

We now consider monochromatic radiation. We can sum any calculated result for the electromagnetic field over frequency components to describe the behavior of complex radiation, once we describe the behavior of monochromatic radiation. We also now restrict ourselves for simplicity to isotropic media, so that, for a given value of ω, the magnitude of the angular wavevector is simply $q = n(\omega)\omega/c$. From Maxwell's equations, we can derive the Helmholtz wave equation that is obeyed by the individual vector components of the electric field $\mathbf{E}(\mathbf{x}, t)$ and magnetic induction $\mathbf{B}(\mathbf{x}, t)$:

$$\left.\begin{aligned} [\nabla^2 + q^2]\mathbf{E}(\mathbf{x}, t) = 0 \\ [\nabla^2 + q^2]\mathbf{B}(\mathbf{x}, t) = 0 \end{aligned}\right\} \quad (9.6)$$

In optical setups, electromagnetic radiation frequently flows past certain regions in one general direction. In other instances, such as when radiation is reflected by a mirror, quantities such as $\mathbf{E}(\mathbf{x}, t)$ can be decomposed into incident and reflected parts, each of which obeys the wave equation and can be considered separately except at the mirror surface. We therefore consider a field $\mathbf{E}(\mathbf{x}, t)$ that is associated with radiation flowing along one general direction.

We next re-express this field as a superposition of spherical waves originating from sources outside the region under consideration. From that, we can show that the electromagnetic energy current density, related to the Poynting vector, is approximately described as a superposition of the squares of the transverse parts of $\mathbf{E}(\mathbf{x}, t)$ associated with both polarizations.

For each polarization state, the energy density W and energy current density $\mathbf{J}$ can be reasonably modeled in terms of a fictitious scalar wave field, $U(\mathbf{x}, t)$. For the case of monochromatic scalar radiation, this field also obeys the Helmholtz wave equation,

$$[\nabla^2 + q^2]U(\mathbf{x}, t) = 0 \tag{9.7}$$

In a given region, if the energy density is $W = C|U(\mathbf{x}, t)|^2$, where C is a scaling constant, the energy current density would be $\mathbf{J} = [c/(n(\omega)q)] \mathrm{Re}\{CU^*(\mathbf{x}, t)\nabla U(\mathbf{x}, t)\}$. An asterisk denotes complex conjugation, and "Re" indicates the real part of an expression. For radiation that is nominally propagating along the direction $\hat{\mathbf{e}}$, we have $\mathbf{J} \cong (cW/n(\omega))\hat{\mathbf{e}}$. This means that the irradiance at a surface can be approximated as being proportional to the time-averaged part of W associated with an incident wave.

9.2.2 Kirchhoff's Integral Formula

Instead of solving the Helmholtz wave equation completely for the scalar radiation field, Kirchhoff (see [4], pp. 427–429, [6]) solved this equation approximately, as a boundary-value problem using Green's function techniques. One Green's function for the Helmholtz equation, once the value of q is assumed, is

$$G(\mathbf{x}, \mathbf{x}') = \frac{\exp(\mathrm{i}q|\mathbf{x} - \mathbf{x}'|)}{|\mathbf{x} - \mathbf{x}'|} \tag{9.8}$$

This Green's function obeys the inhomogeneous equation,

$$(\nabla^2 + q^2)G(\mathbf{x}, \mathbf{x}') = -4\pi\delta^3(\mathbf{x} - \mathbf{x}') \tag{9.9}$$

Here the Laplacian is taken with respect to the first argument, and the Dirac delta function is used, with $\delta^3(\mathbf{x} - \mathbf{x}') = \delta(x - x')\delta(y - y')\delta(z - z')$. We henceforth suppress time dependence for monochromatic radiation, so that $U(\mathbf{x}, t) = U(\mathbf{x})\mathrm{e}^{-\mathrm{i}\omega t}$ is abbreviated as $U(\mathbf{x})$. The problem to be solved to find $U(\mathbf{x})$ is illustrated with the aid of Figure 9.1. The figure shows a cut-away view of Ω, a region of three-dimensional space enclosed by a two-dimensional boundary surface, Q. Radiation is not emitted anywhere within Ω, but it can enter Ω through an aperture whose area Ap lies on Q. Ap can be the surface of a mirror, aperture or lens, and can be flat or curved.

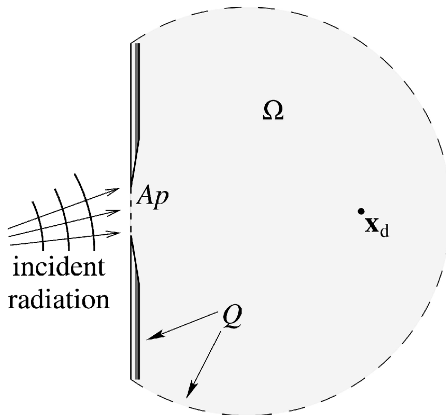

FIG. 9.1. Generic context of Kirchhoff boundary-value problem.

The value $U(\mathbf{x})$ and inwardly directed normal derivative of $U(\mathbf{x})$, $\partial U(\mathbf{x})/\partial n$, are assumed to be equal to the value and normal derivative of an incident wave on Ap, respectively denoted by $U_{\mathrm{i}}(\mathbf{x})$ and $\partial U_{\mathrm{i}}(\mathbf{x})/\partial n$, and to be equal to zero everywhere else on Q. If we set $\mathbf{x}' = \mathbf{x}_{\mathrm{d}}$, where $\mathbf{x}_{\mathrm{d}}$ is a point of interest in Ω, multiplication of Eq. (9.7) on the left by $G(\mathbf{x}, \mathbf{x}_{\mathrm{d}})$ and integration with respect to $\mathbf{x}$ throughout Ω gives

$$\int_{\Omega} \mathrm{d}^3\mathbf{x} G(\mathbf{x}, \mathbf{x}_{\mathrm{d}})(\nabla^2 + k^2)U(\mathbf{x}) = 0 \tag{9.10}$$

Similarly, multiplication of Eq. (9.8) on the left by $U(\mathbf{x})$ and the same integration gives

$$\int_{\Omega} \mathrm{d}^3\mathbf{x} U(\mathbf{x})(\nabla^2 + q^2)G(\mathbf{x}, \mathbf{x}_{\mathrm{d}}) = -4\pi U(\mathbf{x}_{\mathrm{d}}) \tag{9.11}$$

Subtracting Eq. (9.11) from Eq. (9.10) and application of Green's theorem with the assumed boundary conditions gives

$$\begin{aligned} U(\mathbf{x}_{\mathrm{d}}) &= \frac{1}{4\pi}\int_{\Omega} \mathrm{d}^3\mathbf{x}[G(\mathbf{x}, \mathbf{x}_{\mathrm{d}})(\nabla^2 + q^2)U(\mathbf{x}) - U(\mathbf{x})(\nabla^2 + q^2)G(\mathbf{x}, \mathbf{x}_{\mathrm{d}})] \\ &= \frac{1}{4\pi}\int_{\Omega} \mathrm{d}^3\mathbf{x}\{\nabla \cdot [G(\mathbf{x}, \mathbf{x}_{\mathrm{d}})\nabla U(\mathbf{x}) - U(\mathbf{x})\nabla G(\mathbf{x}, \mathbf{x}_{\mathrm{d}})]\} \\ &= \frac{1}{4\pi}\int_{Q} \mathrm{d}^2\mathbf{x}[U(\mathbf{x})\partial G(\mathbf{x}, \mathbf{x}_{\mathrm{d}})/\partial n - G(\mathbf{x}, \mathbf{x}_{\mathrm{d}})\partial U(\mathbf{x})/\partial n] \\ &\cong \frac{1}{4\pi}\int_{Ap} \mathrm{d}^2\mathbf{x}[U_{\mathrm{i}}(\mathbf{x})\partial G(\mathbf{x}, \mathbf{x}_{\mathrm{d}})/\partial n - G(\mathbf{x}, \mathbf{x}_{\mathrm{d}})\partial U_{\mathrm{i}}(\mathbf{x})/\partial n] \end{aligned} \tag{9.12}$$

The fact that contributions from every part of Q other than Ap can be neglected requires more discussion than we provide here. This detail is available, for instance, in Born and Wolf [7].

From Eq. (9.12), we see that, if values are known or at least assumed for $U_{\mathrm{i}}(\mathbf{x})$ and $\partial U_{\mathrm{i}}(\mathbf{x})/\partial n$ on a given optical element, we can find $U(\mathbf{x}_{\mathrm{d}})$ and its derivatives anywhere within Ω. We can use Eq. (9.12) to find $U(\mathbf{x}_{\mathrm{d}})$ and its derivatives on the *next* optical surface (or aperture area) downstream from Ap, by temporarily considering the next element as being within Ω. Repeated, iterative application of Eq. (9.12) in this fashion can help trace the flow of radiation through an optical setup. In many cases, we can assume that the radiation field originates as the radiation from infinitely many mutually incoherent point sources located on the area of a source. Radiation originating at $\mathbf{x}_{\mathrm{s}}$ initially has the form $U(\mathbf{x}) = U_0 \exp(iq\,|\mathbf{x} - \mathbf{x}_{\mathrm{s}}|)/|\mathbf{x} - \mathbf{x}_{\mathrm{s}}|$.

It is probably safe to say that all or nearly all analyses of diffraction effects in radiometry are equivalent to some application of Eq. (9.12). Diffraction effects on the irradiance on a detector area can be inferred from how the value of W or $\mathbf{J}$ computed according to Eq. (9.12) differs from the "ideal" value. The ideal value can be related to the distribution of rays traced from the source through the optical system according to geometrical optics that are incident on a given area. Perfect focusing as found in geometrical optics can lead to infinite ray densities at various places. It is for this reason that the distribution of incident rays can be most safely described in fashions such as the quantity of rays falling on a finite area.

9.2.2.1 Some outstanding issues

The last step in Eq. (9.12) is not rigorous, because the assumed boundary conditions are arbitrary. In fact, it can even be shown that if any solution of the Helmholtz equation $U(\mathbf{x})$ and its normal derivative $\partial U(\mathbf{x})/\partial n$ are both zero everywhere on a finite surface such as the portion of Q other than Ap, then $U(\mathbf{x})$ must be zero everywhere in Ω (see [4], pp. 429–432).

One class of remedies to this problem is to change the boundary conditions, such as by assuming that only a certain linear combination $\alpha U(\mathbf{x}) + \beta \partial U(\mathbf{x})/\partial n$ is known on Q. This leads to the Rayleigh–Sommerfeld variants of the Kirchhoff diffraction theory [8]. This class of remedies requires different Green's functions involving image sources within Ω that help satisfy the assumed boundary conditions. Such Green's functions cannot be found in all instances, but have been formulated for planar Ap. The boundary-diffraction wave (BDW) formulation that is discussed in Section 9.2.3 has been generalized to several boundary conditions and several different types of incident wave fronts on a planar Ap. (Introducing curvature of *Ap* can be similar to warping wave fronts by means of adjusting their phase on a fixed, planar *Ap*.)

More rigorous theoretical treatments of diffraction have also been carried out. Sommerfeld considered diffraction of s- and p-polarized light at the straight edge of an infinitely conducting half-plane [9]. Bethe [10] and Bouwkamp [11] pioneered diffraction by very small, circular holes in perfectly conducting planes, and Levine and Schwinger [12] have carried out related investigations. Braunbek [13] has also attempted to refine Kirchhoff's theory, and Mielenz [14] has recently pursued a rigorous investigation of diffraction effects in close proximity to an aperture and transmission functions of small apertures reminiscent of the work by Levine and Schwinger. There have been other investigations as well, many of which have been compiled by Oughstun [15].

The above investigations lead to two main conclusions that summarize the state of affairs for most diffraction effects in radiometry. First, despite any formal mathematical inconsistencies, the Kirchhoff, Rayleigh–Sommerfeld and more rigorous treatments often predict similar diffraction effects, especially if one is considering a radiation field far from *Ap* and along a direction nearly normal to *Ap* and not too different from the natural path of geometrical rays. Fortunately, this qualification is met in most instances in practical radiometry.

Second, the Kirchhoff theory is bound to break down in the case of very small apertures, if the aperture diameter is at most a few times larger than the wavelength. Exactly how this breakdown occurs remains a problem of theoretical and experimental interest, especially when very small apertures are used in far-infrared measurements. At the time of this writing, measurement uncertainties remain too large to definitively assess the breakdown of Kirchhoff's theory. These uncertainties can have causes ranging from mundane problems such as measurement noise and limited repeatability to issues as fundamental as the ambiguity of what defines an aperture's edge and corresponding area, finite aperture thickness, and imprecise knowledge of appropriate boundary conditions for real apertures.

9.2.3 Boundary-Diffraction-Wave Formulation

Maggi [16], Rubinowicz [17] and Miyamoto and Wolf [18] pioneered a reformulation of Eq. (9.12) that re-expresses the radiation field in the following fashion:

$$U(\mathbf{x}) = U_{\mathrm{G}}(\mathbf{x}) + U_{\mathrm{B}}(\mathbf{x}) \tag{9.13}$$

The first term is called the "geometrical wave." It is the continuation of the wave incident on *Ap* in the illuminated region of Ω and zero in the shadow region. Therefore, $U_G(\mathbf{x})$ and $U_B(\mathbf{x})$ have canceling discontinuities at the boundary between the illuminated and shadow regions. These regions are indicated in Figure 9.2 for several incident waves. The second term is called the BDW, because it re-expresses diffraction effects on $U(\mathbf{x})$ as a line integral around Γ, the perimeter of Ap.

Formulas for $U_B(\mathbf{x})$ vary depending on the incident wavefront [19]. As an example, we can consider the case illustrated in Figure 9.3. If the incident

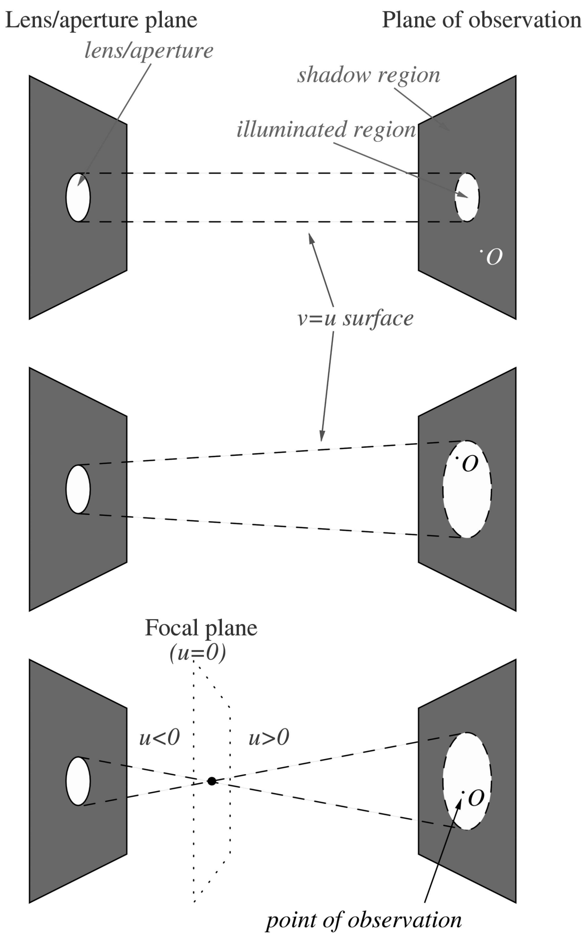

Fig. 9.2. Illuminated and shadow regions for radiation that is a plane wave, diverging spherical wave and converging spherical wave downstream from a lens or aperture. Dashed lines indicate boundary between regions. Cross sections of regions are illustrated in the plane of observation.

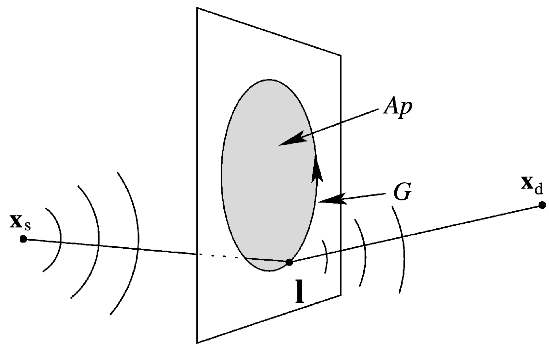

FIG. 9.3. Geometrical construction for BDW formulation.

wave is a spherical wave originating from point $\mathbf{x}_s$ as the spherical wave

$$U_i(\mathbf{x}) = U_0\left(\frac{\exp(iq|\mathbf{x}-\mathbf{x}_s|)}{|\mathbf{x}-\mathbf{x}_s|}\right) \tag{9.14}$$

one has $U_G(\mathbf{x}_d) = U_i(\mathbf{x}_d)$ in the illuminated region, $U_G(\mathbf{x}_d) = 0$ in the shadow region, and

$$U_B(\mathbf{x}_d) = \frac{U_0}{4\pi}\oint_\Gamma \frac{d\mathbf{l}\cdot(\mathbf{d}\times\mathbf{s})}{ds+\mathbf{d}\cdot\mathbf{s}}\left(\frac{\exp(iqs)}{s}\right)\left(\frac{\exp(iqd)}{d}\right) \tag{9.15}$$

Here $\mathbf{l}$ is a point on Γ, we have $\mathbf{d} = \mathbf{l} - \mathbf{x}_d$ and $\mathbf{s} = \mathbf{l} - \mathbf{x}_s$, and the line integral is performed in the right-hand sense about the forward direction of propagation. Besides being easier to evaluate numerically than a double integral, the single integral in Eq. (9.15) also provides better insight into the behavior and asymptotic properties of the BDW. The integrand in Eq. (9.15) has singularities when $\mathbf{x}_d$ is near a geometrical shadow boundary. This requires special care by the practitioner, and points to certain difficulties with the BDW formulation.

9.2.4 Geometrical Theory of Diffraction

Keller and co-workers [20] largely spawned the field of the geometrical theory of diffraction (GTD) in a classic series of papers in 1960s. Two classic volumes on this are the volumes by James [21] and by Borovikov [22]. In a sense, the GTD picture gives results that bear strong similarity to what would result from evaluating the BDW using asymptotic methods such as the stationary-phase approximation to evaluate the line integral. The GTD models the radiation that reaches $\mathbf{r}_d$ as corresponding to a geometrical ray and/or very few rays that are bent at certain points on aperture edges and other places. In geometrical optics, Fermat's least-time principle dictates the path taken by a ray through an optical system. Likewise, the stationary nature of the total optical path length at points on edges in the BDW integrand can be deduced from a generalization of Fermat's principle to the diffracted part of a radiation field.

If we go one step beyond the GTD, continuing to work backwards from solving the full Maxwell's equations with all boundary conditions, one logical finishing point would be to arrive at geometrical optics. Luneburg [23] has presented a systematic development of the successive steps and approximations that can bridge Maxwell's equations and geometrical optics. Luneburg's contribution provides a nearly seamless path from fundamental physical equations to geometrical optics. A similar critique of logical steps and approximations made at each stage might provide insight into future practical approximations describing diffraction effects in radiometry.

9.3 Practical Diffraction Calculations

The Kirchhoff diffraction theory is usually adequate for estimating diffraction effects in radiometry. We can make several additional, simplifying, mathematical approximations to streamline analytic and numerical calculations without significant loss of accuracy. In this section, we discuss some of these approximations, including those related to Gaussian optics and developments that lead to the Fraunhofer and Fresnel approximations.

9.3.1 Unfolding and Neglect of Obliquity Factors

Note how the optical setup in Figure 9.4a can be "unfolded" into a nearly equivalent optical system shown in Figure 9.4b, with the following characteristics: a length that is much larger than its width, and radiation that is incident on or proceeds downstream from surfaces of optical elements (including aperture areas) at angles close to normal. This justifies using the following approximations in Eq. (9.12):

$$\frac{\partial G(\mathbf{x}, \mathbf{x}_\mathrm{d})}{\partial n} \cong -\mathrm{i}qG(\mathbf{x}, \mathbf{x}_\mathrm{d}) \tag{9.16}$$

and

$$\frac{\partial U_\mathrm{i}(\mathbf{x})}{\partial n} \cong +\mathrm{i}qU_\mathrm{i}(\mathbf{x}) \tag{9.17}$$

Hence, Eq. (9.12) can be rewritten as

$$U(\mathbf{x}_\mathrm{d}) \cong \frac{1}{\mathrm{i}\lambda}\int_{Ap} \mathrm{d}^2\mathbf{x}\, U_\mathrm{i}(\mathbf{x})G(\mathbf{x}, \mathbf{x}_\mathrm{d}) \tag{9.18}$$

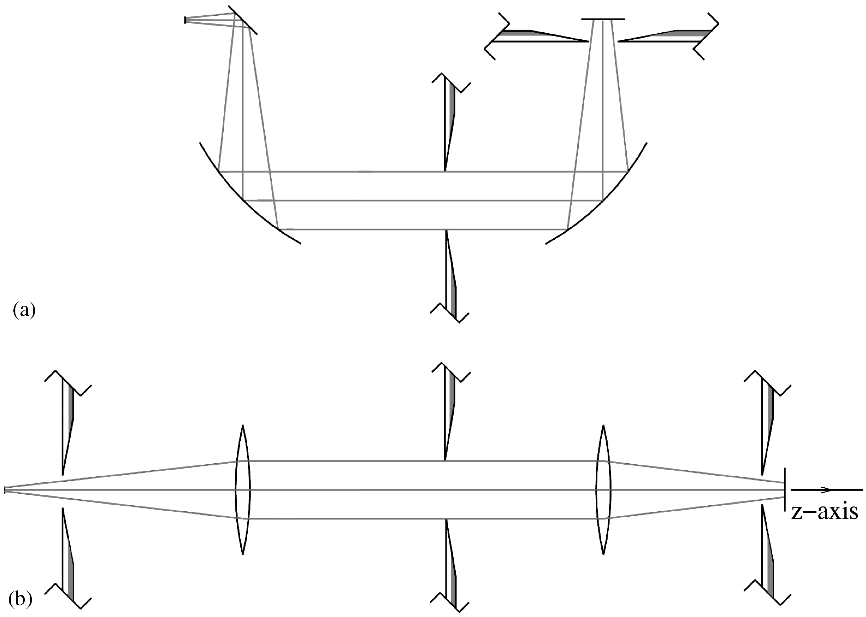

FIG. 9.4. Unfolding of an optical setup: (a) actual setup, (b) unfolded setup.

9.3.2 Gaussian-Optics Approximation of a Spherical Wave

The Green's function given in Eq. (9.8) has the form of a spherical wave that involves the distance between $\mathbf{x}$ and $\mathbf{x}'$ in the exponent and in the denominator. This distance can be expanded in a Taylor expansion,

$$\begin{aligned} \left|\mathbf{x} - \mathbf{x}'\right| &= [(x - x')^2 + (y - y')^2 + (z - z')^2]^{1/2} \\ &= \left|z - z'\right| + \frac{(x - x')^2 + (y - y')^2}{2|z - z'|} + \cdots \\ &\cong \left|z - z'\right| + \left(\frac{x^2 + y^2}{2|z - z'|}\right) + \left(\frac{x'^2 + y'^2}{2|z - z'|}\right) - \left(\frac{xx' + yy'}{|z - z'|}\right) \end{aligned} \tag{9.19}$$

As shown in Figure 9.4b, the z-axis is the optical axis of the unfolded setup, with propagation generally along the positive-z direction. The Taylor expansion in Eq. (9.19) assumes that distances along the z-axis between points on successive optical elements are much larger than the corresponding distances along transverse directions.

In Gaussian or paraxial optics, a distance in the exponent is approximated by the four terms shown in Eq. (9.19), but a distance in the denominator is approximated by the first term only:

$$G(\mathbf{x}, \mathbf{x}') \cong \frac{\exp\left\{ \mathrm{i}q\left[|z - z'| + \left(\frac{x^2 + y^2}{2|z - z'|} \right) + \left(\frac{x'^2 + y'^2}{2|z - z'|} \right) - \left(\frac{xx' + yy'}{|z - z'|} \right) \right] \right\}}{|z - z'|} \tag{9.20}$$

This combination of approximations has several advantages. One regarding its efficacy is "self-consistency," which is discussed later. A key practical advantage is that the approximate Green's function is proportional to a generalized Gaussian-type exponential function. We can use this fact to great advantage, because of the insight that is available regarding integration of Gaussian functions. This becomes especially clear when we realize that such integration is done over two-dimensional surfaces. The right-hand side of Eq. (9.20) is the product of four factors: an overall prefactor, a Gaussian that depends on the transverse coordinates x and y on one optical element, a corresponding Gaussian that depends on x' and y', and an exponential function involving the inner product of both sets of transverse coordinates, $xx' + yy'$.

One can also easily include curvature of optical surfaces in Gaussian-optics in an analogous approximate fashion. A curved element is approximated as a thin lens. A ray passing through such an element is treated as a ray passing through a constant-z surface, but with a modified effective optical path length depending on the transverse coordinates x and y where it crosses the surface. This modification is done by the replacement

$$U_{\mathrm{i}}(x, y, z) \to U_{\mathrm{i}}(x, y, z) \exp\left[-\frac{\mathrm{i}q(x^2 + y^2)}{2f} \right] \tag{9.21}$$

after U_{i} is computed and before we iterate Eq. (9.18) to the next element. The parameter f is the signed focal length of the optical element. A non-curved element has $f = \pm\infty$.

9.3.3 Fraunhofer and Fresnel Diffraction

In the case of diffraction of a spherical wave originating at $\mathbf{x}$ by one optical element in free space shown in Figure 9.5, we have

$$\begin{aligned} &U(x', y', z') \\ &\quad \cong \frac{U_0 e^{\mathrm{i}q(d+d')}}{\mathrm{i}\lambda d d'} \iint_{Ap} \mathrm{d}^2\mathbf{x}'' \exp\left\{ \mathrm{i}q \left[\frac{(x - x'')^2 + (y - y'')^2}{2d} \right.\right. \\ &\qquad \left.\left. + \frac{(x' - x'')^2 + (y' - y'')^2}{2d'} - \frac{x''^2 + y''^2}{2f} \right] \right\} \end{aligned} \tag{9.22}$$

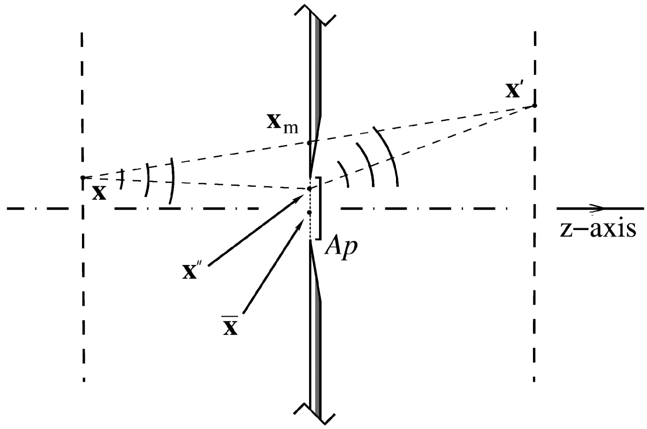

FIG. 9.5. Parameters pertinent to diffraction by a single optical element.

This approximates the initial spherical wave originating at $\mathbf{x}$ and $G(\mathbf{x}'', \mathbf{x}')$ according to Gaussian-optics and allows for focusing effects. It can be rearranged by introducing

$$x_\mathrm{m} = \frac{xd' + x'd}{d + d'}, \qquad y_\mathrm{m} = \frac{yd' + y'd}{d + d'} \tag{9.23}$$

the coefficient

$$C = \frac{1}{2d} + \frac{1}{2d'} - \frac{1}{2f} \tag{9.24}$$

and

$$x'_\mathrm{m} = x_\mathrm{m}\left(1 - \frac{1}{2Cf}\right), \quad y'_\mathrm{m} = y_\mathrm{m}\left(1 - \frac{1}{2Cf}\right) \tag{9.25}$$

If we indicate the distance along the geometrical optical path from $\mathbf{x}$ to $\mathbf{x}'$ as

$$L_0 = d + d' + \frac{(x - x')^2 + (y - y')^2}{2(d + d')} + \frac{x_\mathrm{m}x'_\mathrm{m} + y_\mathrm{m}y'_\mathrm{m}}{2f} \tag{9.26}$$

we have the convenient result,

$$U(x', y', z') \cong \frac{U_0 \mathrm{e}^{\mathrm{i}qL_0}}{\mathrm{i}\lambda dd'} \iint_{Ap} \mathrm{d}x''\mathrm{d}y'' \exp\{\mathrm{i}qC[(x'' - x'_\mathrm{m})^2 + (y'' - y'_\mathrm{m})^2]\} \tag{9.27}$$

Here $(x'' - x'_\mathrm{m}, y'' - y'_\mathrm{m}, 0)$ is the position of a point on the element area Ap relative to $(x'_\mathrm{m}, y'_\mathrm{m}, z'')$. By Fermat's principle, the geometrical optical path from $\mathbf{x}$ to $\mathbf{x}'$ intersects the $z = z''$ plane at $(x'_\mathrm{m}, y'_\mathrm{m}, z'')$.

Consider a point $(\bar{x}, \bar{y}, z'')$ near the center of Ap. Then

$$(x'' - x'_{\mathrm{m}})^2 = [(x'' - \bar{x}) + (\bar{x} - x'_{\mathrm{m}})]^2 = (x'' - \bar{x})^2 + 2(\bar{x} - x'_{\mathrm{m}})(x'' - \bar{x}) + (\bar{x} - x'_{\mathrm{m}})^2$$

and

$$(y'' - y'_{\mathrm{m}})^2 = [(y'' - \bar{y}) + (\bar{y} - y'_{\mathrm{m}})]^2 = (y'' - \bar{y})^2 + 2(\bar{y} - y'_{\mathrm{m}})(y'' - \bar{y}) + (\bar{y} - y'_{\mathrm{m}})^2$$

imply that we have

$$U(x', y', z') \cong \frac{U_0 \mathrm{e}^{\mathrm{i}q\{L_0 + C[(\bar{x} - x'_{\mathrm{m}})^2 + (\bar{y} - y'_{\mathrm{m}})^2]\}}}{\mathrm{i}\lambda d d'} \times \iint_{Ap} \mathrm{d}x'' \mathrm{d}y'' \mathrm{e}^{\mathrm{i}qC[2(\bar{x} - x'_{\mathrm{m}})(x'' - \bar{x}) + 2(\bar{y} - y'_{\mathrm{m}})(y'' - \bar{y}) + (x'' - \bar{x})^2 + (y'' - \bar{y})^2]} \tag{9.28}$$

This involves a prefactor and an integral of an exponential function. The argument in the exponent has terms that are linear and quadratic in $(x'' - \bar{x})$ and $(y'' - \bar{y})$. For a sufficiently small aperture, only the linear terms matter, and $U(x', y', z')$ is proportional to the Fourier transform of a function that is unity on Ap and zero elsewhere. This function is sometimes called the "aperture function." In the Fraunhofer approximation, we keep only the linear terms. In the Fresnel approximation, we keep the linear and quadratic terms. As C approaches zero, which occurs when $\mathbf{x}$ and $\mathbf{x}'$ are in conjugate planes, x'_{m} and y'_{m} diverge proportionally to C^{-1}, and the quadratic terms inside the exponent vanish. Hence, only the linear terms matter. The divergent terms in the exponent in the prefactor all cancel one another when C approaches zero, so that the exponent reaches a limit.

9.3.4 Diffraction Effects for Multiple Elements

If there are multiple optical elements in series between the point $\mathbf{x}_{\mathrm{s}}$ at which radiation is emitted and the point $\mathbf{x}_{\mathrm{d}}$, generalization of the foregoing analysis gives

$$U(\mathbf{x}_{\mathrm{d}}) \cong \frac{U_0 \mathrm{e}^{\mathrm{i}q(d_0 + d_1 + \cdots + d_N)}}{(\mathrm{i}\lambda)^N d_0 d_1 \ldots d_N} \iint_{Ap1} \mathrm{d}x_1 \mathrm{d}y_1 \ldots \iint_{ApN} \mathrm{d}x_N \mathrm{d}y_N \times \exp\left[\mathrm{i}q \sum_{\mu,\nu=0}^{N+1} B_{\mu\nu}(x_\mu x_\nu + y_\mu y_\nu)\right] \tag{9.29}$$

Various parameters are defined as indicated in Figure 9.6. The convention of $(x_{\mathrm{s}}, y_{\mathrm{s}}, z_{\mathrm{s}}) = (x_0, y_0, z_{\mathrm{s}})$ and $(x_{\mathrm{d}}, y_{\mathrm{d}}, z_{\mathrm{d}}) = (x_{N+1}, y_{N+1}, z_{\mathrm{d}})$ is used in the sum in

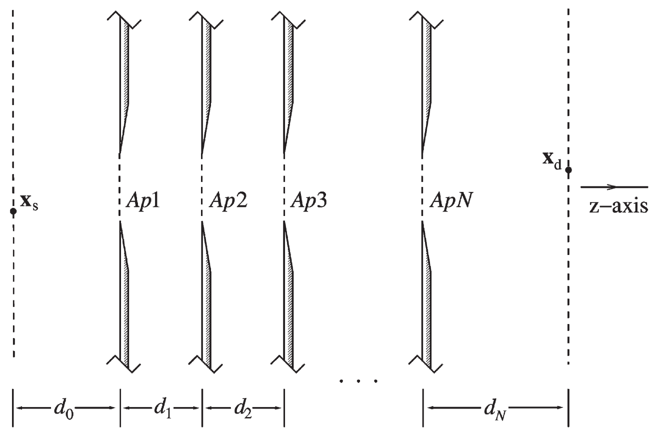

FIG. 9.6. Optical setup with multiple apertures that can diffract radiation in series.

Eq. (9.29), with

$$B_{\mu\nu} = [(d_{\mu-1}^{-1} + d_{\mu}^{-1} - f_{\mu}^{-1})\delta_{\mu\nu} + d_{\mu-1}^{-1}\delta_{\mu-1,\nu} + d_{\mu}^{-1}\delta_{\mu+1,\nu}]/2 \tag{9.30}$$

The Gaussian form of Eq. (9.29) permits progress along analytical and numerical lines regarding diffraction effects in optical systems featuring such a series of elements. Examples of this are provided later.

9.3.5 Self-Consistency of Gaussian-Optics

If we integrate Eq. (9.27) over the entire $z = z''$ plane,

$$\tilde{U}(x', y', z') \cong \frac{U_0 e^{iqL_0}}{i\lambda dd'} \int_{-\infty}^{+\infty} dx'' \int_{-\infty}^{+\infty} dy'' \exp\{iqC[(x'' - x'_m)^2 + (y'' - y'_m)^2]\} \tag{9.31}$$

we obtain the same result as if Ap covered the entire plane. We can evaluate Eq. (9.31) analytically. Explicitly writing the value of C for $f = \pm\infty$ gives

$$\tilde{U}(x', y', z') = \frac{U_0 e^{iqL_0}}{dd'} \left(\frac{1}{d} + \frac{1}{d'}\right)^{-1} = \frac{U_0 e^{iqL_0}}{d + d'} \tag{9.32}$$

and

$$\left|\tilde{U}(x', y', z')\right|^2 = \frac{|U_0|^2}{(d + d')^2} \tag{9.33}$$

Eqs. (9.32) and (9.33) give the same result as would be expected from geometrical optics, so that Fresnel diffraction is "self-consistent" (see [3], pp. 148–152). Changing any interval over which a spherical wave propagates freely into two subintervals on opposite sides of an infinite clear aperture does not change results. It may not be immediately obvious that this "check" works, because Eqs. (9.18) and (9.20) involve three different approximations. However, the combination of all three of these approximations leads to the above self-consistency. There is a further self-consistency of Gaussian-optics in the form of a conservation law. Suppose we take Eq. (9.18) and integrate $|U(\mathbf{x}_\mathrm{d})|^2$ over the entire $z = z_\mathrm{d}$ plane. The result is

$$
\begin{aligned}
&\int_{-\infty}^{+\infty} \mathrm{d}x_\mathrm{d} \int_{-\infty}^{+\infty} \mathrm{d}y_\mathrm{d} \left|U(\mathbf{x}_\mathrm{d})\right|^2 \\
&= \frac{1}{\lambda^2} \int_{-\infty}^{+\infty} \mathrm{d}x_\mathrm{d} \int_{-\infty}^{+\infty} \mathrm{d}y_\mathrm{d} \int_{Ap} \mathrm{d}^2\mathbf{x} \int_{Ap} \mathrm{d}^2\mathbf{x}' [U_\mathrm{i}(\mathbf{x}) G(\mathbf{x}, \mathbf{x}_\mathrm{d})]^* U_\mathrm{i}(\mathbf{x}') G(\mathbf{x}', \mathbf{x}_\mathrm{d}) \\
&= \frac{1}{\lambda^2 d^2} \int_{Ap} \mathrm{d}^2\mathbf{x} \int_{Ap} \mathrm{d}^2\mathbf{x}' [U_\mathrm{i}(\mathbf{x})]^* U_\mathrm{i}(\mathbf{x}') \\
&\quad \times \int_{-\infty}^{+\infty} \mathrm{d}x_\mathrm{d} \int_{-\infty}^{+\infty} \mathrm{d}y_\mathrm{d} \exp\left\{ \frac{\mathrm{i}q[(x' - x_\mathrm{d})^2 - (x - x_\mathrm{d})^2 + (y' - y_\mathrm{d})^2 - (y - y_\mathrm{d})^2]}{2d} \right\} \\
&= \frac{1}{\lambda^2 d^2} \int_{Ap} \mathrm{d}^2\mathbf{x} \int_{Ap} \mathrm{d}^2\mathbf{x}' [U_\mathrm{i}(\mathbf{x})]^* U_\mathrm{i}(\mathbf{x}') \exp\left[\frac{\mathrm{i}q(x'^2 - x^2 + y'^2 - y^2)}{2d} \right] \\
&\quad \times \int_{-\infty}^{+\infty} \mathrm{d}x_\mathrm{d} \exp\left\{ \left[\frac{\mathrm{i}q(x - x')}{d} \right] x_\mathrm{d} \right\} \int_{-\infty}^{+\infty} \mathrm{d}y_\mathrm{d} \exp\left\{ \left[\frac{\mathrm{i}q(y - y')}{d} \right] y_\mathrm{d} \right\} \\
&= \int_{Ap} \mathrm{d}^2\mathbf{x} \int_{Ap} \mathrm{d}^2\mathbf{x}' [U_\mathrm{i}(\mathbf{x})]^* U_\mathrm{i}(\mathbf{x}') \delta(x - x') \delta(y - y')
\end{aligned} \tag{9.34}
$$

or

$$
\int_{-\infty}^{+\infty} \mathrm{d}x_\mathrm{d} \int_{-\infty}^{+\infty} \mathrm{d}y_\mathrm{d} \left|U(\mathbf{x}_\mathrm{d})\right|^2 = \int_{Ap} \mathrm{d}^2\mathbf{x} \left|U_\mathrm{i}(\mathbf{x})\right|^2 \tag{9.35}
$$

Thus, the integrated spectral power falling on the area of one optical element is conserved when it reaches the plane of the next optical element. This implies a transmission function of unity even for very small apertures, which indicates a breakdown of the Kirchhoff diffraction theory in the small-aperture limit. However, this also ensures that the theoretical diffraction effects on total transmitted spectral flux approach zero correctly in the opposite, small-λ limit.

9.3.6 Limitations of Approximations

The Gaussian-optics version of the Kirchhoff diffraction theory is widely found and used in the radiometric literature with good success. This version often predicts diffraction effects very similar to results obtained without making the approximations found in Eqs. (9.18), (9.20) and (9.21).

One should also be mindful of when a Gaussian-optics picture should fail. It breaks down when describing diffraction effects for very small apertures, mainly because the Kirchhoff theory itself breaks down. It does not describe aberrations correctly, so their effects must be otherwise considered. The present Gaussian-optics implementation of the Kirchhoff theory should also break down when obliquity factors become appreciably different from unity or when distances between optical elements do not greatly exceed the wavelength. However, because the correct results are obtained in the limit of optical elements whose areas extend over entire constant-z planes, and because the total integrated flux is conserved in the manner demonstrated above, a Gaussian-optics picture can be useful in many practical situations (for which a cursory assessment of its validity might suggest otherwise).

9.4 The SAD Problem

Even in complicated optical setups, diffraction effects can arise mainly from one optical element. In other setups, the effects might be approximately described as the sum of effects of several different elements considered individually. In either type of situation, diffraction effects on the throughput of an optical system can be related to the diffraction effects that would occur in fictitious three-element setups that consist of an extended Lambertian *source*, *aperture* and *detector*. Such setups and the related diffraction problem may be denoted by the acronym, SAD. The SAD problem is one of the most studied diffraction problems in optics and radiometry. Furthermore, its study has been very profitable.

Consider the setup illustrated in Figure 9.7(a). A blackbody cavity placed behind a defining aperture illuminates a detector. To reduce the stray light reaching the detector, two non-limiting apertures are also placed strategically between the defining aperture and detector. Three SAD combinations are shown in Figure 9.7(b)–(d). Appropriate combination of diffraction effects arising in cases of the fictitious combinations of three indicated elements can account reasonably well for overall diffraction effects in the real setup with relatively little effort. In Figure 9.7(b), the defining aperture limits the throughput of the model optical system. In Figure 9.7(c) and (d), the non-limiting apertures would tend to increase the throughput of the model optical systems. For the non-limiting apertures, the effective source is the defining aperture. Depending on the geometry and wavelength, the sum of all diffraction effects can lead to a throughput that is smaller or larger than that expected geometrically.

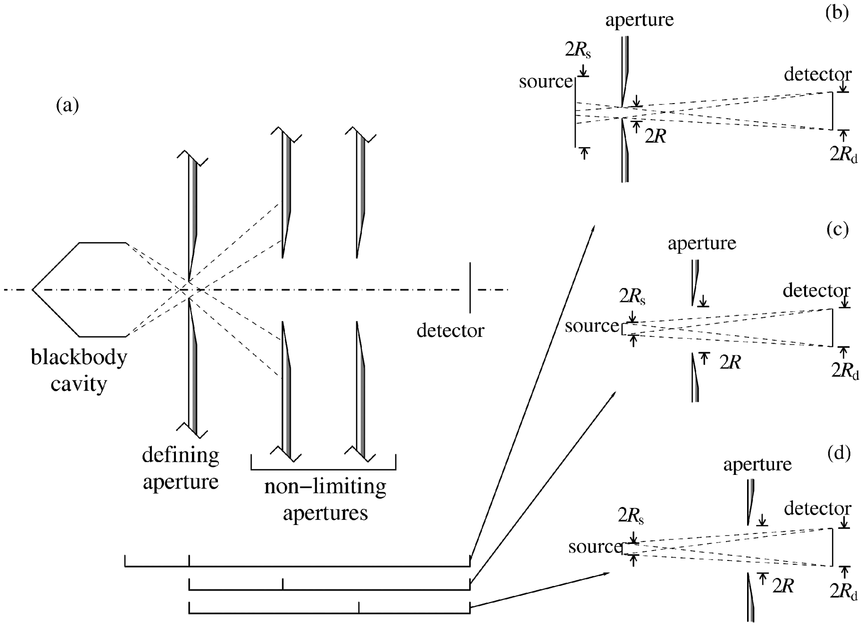

FIG. 9.7. Optical setup conceptually treated as three SAD setups for purposes of diffraction effects.

9.4.1 Lommel's Treatment for a Point Source

The ratio $U(x', y', z')/U_0$ implied by Eq. (9.28) is a function of x'_m and y'_m symmetric with respect to simultaneous exchange $\mathbf{x}$ with $\mathbf{x}'$ and d with d':

$$\frac{U(x', y', z')}{U_0} = S(x'_m, y'_m) = \frac{e^{iqL_0}}{i\lambda dd'} \iint_{Ap} dx'' dy'' e^{iqC[(x''-x'_m)^2 + (y''-y'_m)^2]} \tag{9.36}$$

We now assume that Ap is circular with radius R and centered on the z-axis. Introducing polar coordinates, $r'' = (x''^2 + y''^2)^{1/2}$, $r' = (x'^2_m + y'^2_m)^{1/2}$, and θ, the relative polar angle between (x'', y'') and (x'_m, y'_m), we obtain

$$S(x'_m, y'_m) = S(r') = \frac{e^{iqL_0}}{i\lambda dd'} \int_0^R dr'' r'' \int_0^{2\pi} d\theta e^{iqC(r''^2 + r'^2 - 2r''r' \cos\theta)} \tag{9.37}$$

In the $q \to \infty$ limit, we have $S(r') \sim S_G(r')$, with

$$S_G(r') = \frac{e^{iqL_0}\Theta(R/r' - 1)}{2dd'C} \tag{9.38}$$

Here $\Theta(x)$ is the Heaviside step function.

Introducing the unit-less parameters $\rho = r''/R$ (which varies from 0 to 1 on Ap), $u = 2qCR^2$, and $v = \left|2qCRr'\right|$, we have

$$S(r') = \frac{R^2 \exp[\mathrm{i}q(L_0 + Cr'^2)]}{\mathrm{i}\lambda dd'} \int_0^1 \mathrm{d}\rho\rho \int_0^{2\pi} \mathrm{d}\theta \mathrm{e}^{\mathrm{i}u\rho^2/2 - \mathrm{i}v\rho\cos\theta} \tag{9.39}$$

Lommel showed that the above integrals can be expressed using Neumann series' of Bessel functions [24], and the resulting functions are traditionally called Lommel functions of two arguments. Lommel's treatment is also given by Born and Wolf (see [7], pp. 435–442). Here, the quantity of greatest interest is the squared ratio, $\left|S(r')/S_{\mathrm{G}}(0)\right|^2$. The quantity $\left|S(r')/S_{\mathrm{G}}(0)\right|^2 - 1$ gives the diffraction effects on point-to-point propagation of radiation, normalized so that the geometrically allowed propagation is unity.

The Lommel functions are

$$U_n(u, v) = \sum_{s=0}^{\infty} (-1)^s (u/v)^{n+2s} J_{n+2s}(v) \tag{9.40}$$

and

$$V_n(u, v) = \sum_{s=0}^{\infty} (-1)^s (v/u)^{n+2s} J_{n+2s}(v) \tag{9.41}$$

where n is an integer. $U_n(u, v)$ and $V_n(u, v)$ can be related to each other by $U_n(u, v) = V_n(v^2/u, v)$ and $V_n(u, v) = U_n(v^2/u, v)$. These functions also have other useful symmetries, including $U_n(u, v) = U_n(u, -v)$, $V_n(u, v) = V_n(u, -v)$, $U_n(u, v) = (-1)^n U_n(-u, v)$, and $V_n(u, v) = (-1)^n V_n(-u, v)$. Recent algorithms to evaluate Lommel functions of two arguments efficiently and to varying degrees of accuracy are described by Mielenz [25], Shirley and Terraciano [26], Shirley and Chang [27], and Edwards and McCall [28].

It is traditional to express the value of $\left|S(r')/S_{\mathrm{G}}(0)\right|^2$ using either of two equivalent formulas:

$$\left|\frac{S(r')}{S_{\mathrm{G}}(0)}\right|^2 = U_1^2(u, v) + U_2^2(u, v) \tag{9.42}$$

or

$$\left|\frac{S(r')}{S_{\mathrm{G}}(0)}\right|^2 = 1 + V_0^2(u, v) + V_1^2(u, v) - 2V_0(u, v)\cos\left[\frac{1}{2}\left(v + \frac{u^2}{v}\right)\right] - 2V_1(u, v)\sin\left[\frac{1}{2}\left(v + \frac{u^2}{v}\right)\right] \tag{9.43}$$

Equation (9.42) tends to be more convenient if the geometrical optical path between $\mathbf{x}$ and $\mathbf{x}'$ is obstructed (which implies $r' > R$). Equation (9.43) tends to be more convenient if that path is not blocked (which implies $r' < R$).

In the BDW formulation, when we have $r' > R$, the combination $U_1^2(u,v) + U_2^2(u,v)$ on the right-hand side of Eq. (9.42) results from the square of the BDW U_B. Likewise, when we have $r' < R$, the leading "1" on the right-hand side of Eq. (9.43) results from the square of the geometrical wave U_G, $V_0^2(u,v) + V_1^2(u,v)$ results from the square of U_B, and the remaining terms result from interference of U_G with U_B.

9.4.1.1 Asymptotic properties of Lommel's result

In the small-λ regime, when the geometrical optical path between $\mathbf{x}$ and $\mathbf{x}'$ is not blocked, the asymptotic behavior of Bessel functions of a large positive argument,

$$J_m(v) \sim \left(\frac{2}{\pi v}\right)^{1/2} \cos(v - m\pi/2 - \pi/4) \tag{9.44}$$

gives

$$V_0(u,v) \cong \left(\frac{2}{\pi v}\right)^{1/2} \frac{\cos(v - \pi/4)}{1 - v^2/u^2} \tag{9.45}$$

and

$$V_1(u,v) \cong \left(\frac{2}{\pi v}\right)^{1/2} \left(\frac{v}{u}\right) \frac{\sin(v - \pi/4)}{1 - v^2/u^2} \tag{9.46}$$

Substitution of these approximations into Eq. (9.43) gives

$$\begin{aligned}\left|\frac{S(r')}{S_G(0)}\right|^2 \cong\ & 1 + \frac{1}{\pi v}\left[\frac{1 + v^2/u^2}{(1 - v^2/u^2)^2}\right] + \frac{1}{\pi v}\left[\frac{\sin(2v)}{1 - v^2/u^2}\right] - \left(\frac{2}{\pi v}\right)^{1/2} \\ & \times \left\{\frac{\cos[(u+v)^2/(2u) - \pi/4]}{1 + v/u} + \frac{\cos[(u-v)^2/(2u) + \pi/4]}{1 - v/u}\right\}\end{aligned} \tag{9.47}$$

When the geometrical optical path is blocked, we have

$$U_1(u,v) \cong \left(\frac{2}{\pi v}\right)^{1/2} \left(\frac{u}{v}\right) \frac{\sin(v - \pi/4)}{1 - u^2/v^2} \tag{9.48}$$

$$U_2(u,v) \cong -\left(\frac{2}{\pi v}\right)^{1/2} \left(\frac{u}{v}\right)^2 \frac{\cos(v - \pi/4)}{1 - u^2/v^2} \tag{9.49}$$

and

$$\left|\frac{S(r')}{S_G(0)}\right|^2 \cong \frac{u^2}{\pi v^3}\left[\frac{1 + u^2/v^2}{(1 - u^2/v^2)^2}\right] - \frac{u^2}{\pi v^3}\left[\frac{\sin(2v)}{1 - u^2/v^2}\right] \tag{9.50}$$

While Eqs. (9.42) and (9.43) are formally equivalent, the asymptotic approximation being used here requires that Eq. (9.47) or Eq. (9.50) is used only in the respective case of non-blockage or blockage of the geometrical optical path from $\mathbf{x}$ to $\mathbf{x}'$. In each case, Eq. (9.47) or (9.50) breaks down as r' approaches R.

Equations (9.47) and (9.50) illustrate the main behavior of diffraction effects on point-to-point propagation of radiation using simple functions. These equations contain both non-oscillatory and oscillatory terms. The non-oscillatory terms often matter the most. Cumulative effects of oscillatory terms can be largely self-canceling upon $\mathbf{x}$ sampling the source area, such as in the case of an extended source, $\mathbf{x}'$ sampling the finite detector area, and/or λ sampling the relevant spectrum in the case of complex radiation.

9.4.2 Wolf's Formula for Integrated Flux

Wolf [29] introduced the function, $L(u, v_0)$, which is the fraction of the flux that is incident on Ap that subsequently falls on a circular area A' of the $z = z'$ plane. For all points $\{\mathbf{x}'\}$ on A', we have $v < v_0$, and we have $v = v_0$ for points on the perimeter of A'. In analogy with Lommel's result, $L(u, v_0)$ can be given by one expression that is more convenient when the geometrical optical paths between points on the perimeter of A' and $\mathbf{x}$ are blocked, implying $v_0 > |u|$, and by a different expression that is more convenient when these paths are not blocked, implying $v_0 < |u|$. First, we introduce the functions,

$$Q_{2s}(v_0) = \sum_{p=0}^{2s} (-1)^p [J_p(v_0) J_{2s-p}(v_0) + J_{p+1}(v_0) J_{2s+1-p}(v_0)] \tag{9.51}$$

and

$$Y_n(u, v_0) = \sum_{s=0}^{\infty} (-1)^s (n + 2s)(v_0/u)^{n+2s} J_{n+2s}(v_0) \tag{9.52}$$

For $v_0 > |u|$, we have

$$L(u, v_0) = 1 - \sum_{s=0}^{\infty} \frac{(-1)^s}{2s+1} \left(\frac{u}{v_0}\right)^{2s} Q_{2s}(v_0) \tag{9.53}$$

For $v_0 < |u|$, we have

$$\begin{aligned} L(u, v_0) = {} & \left(\frac{v_0}{u}\right)^2 \left[1 + \sum_{s=0}^{\infty} \frac{(-1)^s}{2s+1} \left(\frac{v_0}{u}\right)^{2s} Q_{2s}(v_0)\right] \\ & - \frac{4}{u} \left\{ Y_1(u, v_0) \cos\left[\frac{1}{2}\left(u + \frac{v_0^2}{u}\right)\right] \right. \\ & \left. + Y_2(u, v_0) \sin\left[\frac{1}{2}\left(u + \frac{v_0^2}{u}\right)\right] \right\} \end{aligned} \tag{9.54}$$

This formula is typeset incorrectly in several editions of Born and Wolf's classic text.

9.4.2.1 Asymptotic properties of Wolf's result

Focke [30] considered the asymptotic properties of the above integrated flux, based on work by Schwarzschild [31], van Kampen [32] and Wolf's treatment, and obtained

$$L(u, v_0) \sim 1 - \frac{2}{\pi}\left(\frac{v_0}{v_0^2 - u^2}\right) \tag{9.55}$$

which is valid for large v_0 subject to having $v_0 > |u|$.

One may also consider the more general asymptotic expansion for a Bessel function of large non-negative argument [33],

$$J_m(v) \sim \left(\frac{2}{\pi v}\right)^{1/2}\left[\cos\zeta \sum_{s=0}^{\infty} \frac{(-1)^s A_{2s}(m)}{v^{2s}} - \sin\zeta \sum_{s=0}^{\infty} \frac{(-1)^s A_{2s+1}(m)}{v^{2s+1}}\right] \tag{9.56}$$

with $\zeta = v - m\pi/2 - \pi/4$, $A_0(m) = 1$, and $A_s(m) = (4m^2 - 1^2)(4m^2 - 3^2)\cdots [4m^2 - (2s-1)^2]/[8^s(s!)]$ for all other s, and apply this approximation to Wolf's result. For $|w| < 1$, this gives

$$\begin{aligned}\sum_{s=0}^{\infty} \frac{(-1)^s}{2s+1} w^{2s} Q_{2s}(v) = {} & \frac{2\sigma_0}{\pi v} - \frac{\sigma_0 \cos(2v)}{\pi v^2} \\ & - \frac{16\sigma_4 + 32\sigma_3 + 8\sigma_2 - 8\sigma_1 - 3\sigma_0}{12\pi v^3} \\ & + \left(\frac{8\sigma_2 + 8\sigma_1 - \sigma_0}{4\pi v^3}\right)\sin(2v) \\ & + \left(\frac{64\sigma_4 + 128\sigma_3 - 16\sigma_2 - 80\sigma_1 + 9\sigma_0}{32\pi v^4}\right) \\ & \times \cos(2v) + O(v^{-5})\end{aligned} \tag{9.57}$$

The σ_k parameters are defined by

$$\sigma_k = \sum_{s=0}^{\infty} s^k w^{2s} = \left(w^2 \frac{\mathrm{d}}{\mathrm{d}(w^2)}\right)^k \frac{1}{1 - w^2} = \frac{W_k(w^2)}{(1 - w^2)^{k+1}} \tag{9.58}$$

The first six W-polynomials are

$$\begin{gathered} W_0(x) = 1, W_3(x) = x^3 + 4x^2 + x, \\ W_1(x) = x, W_4(x) = x^4 + 11x^3 + 11x^2 + x, \\ W_2(x) = x^2 + x, W_5(x) = x^5 + 26x^4 + 66x^3 + 26x^2 + x \end{gathered} \tag{9.59}$$

Application of Eq. (9.56) also gives

$$
\begin{aligned}
Y_1(u,v) = \frac{v^2}{2u}\left(\frac{2}{\pi v}\right)^{1/2} \Bigg[& \left(\frac{2\sigma_0 + 4\sigma_1}{v}\right)\sin(v-\pi/4) \\
& + \left(\frac{3\sigma_0 + 22\sigma_1 + 48\sigma_2 + 32\sigma_3}{4v^2}\right)\cos(v-\pi/4) \\
& + \left(\frac{15\sigma_0 + 62\sigma_1 - 160\sigma_2 - 960\sigma_3 - 1280\sigma_4 - 512\sigma_5}{64v^3}\right) \\
& \times \sin(v-\pi/4)\Bigg] + O(v^{-7/2})
\end{aligned}
\tag{9.60}
$$

and

$$
\begin{aligned}
Y_2(u,v) = -\frac{v}{2}\left(\frac{2}{\pi v}\right)^{1/2} & \left[\left(\frac{4\sigma_1}{v}\right)\sin(v+\pi/4) + \left(\frac{-\sigma_1 + 16\sigma_3}{2v^2}\right)\cos(v+\pi/4)\right. \\
& \left. + \left(\frac{-9\sigma_1 + 160\sigma_3 - 256\sigma_5}{32v^3}\right) \times \sin(v+\pi/4)\right] + O(v^{-7/2})
\end{aligned}
\tag{9.61}
$$

As mentioned earlier and as noted by Focke, oscillatory terms can be less relevant and even undesirable to include when considering diffraction effects, because they can be self-canceling upon spatial or spectral integration, and when sampled at discrete wavelengths they can lead to randomly biased results.

9.4.3 Diffraction Effects on Spectral Throughput

The above analysis lays the groundwork for estimating diffraction effects on spectral throughput of optical systems. In this Section, we show how this is done for the SAD problem and its application to treat systems with varying degrees of complexity.

9.4.3.1 SAD case

The preceding analysis considered flux arising from a point source, but the finite extent of the source may also need to be taken into account. It is helpful to introduce the parameters, $v_s = qR_sR/d$, $v_d = qR_dR/d'$, $v_M = \max(v_s, v_d)$, and $\sigma = \min(v_s, v_d)/\max(v_s, v_d)$. R_s and R_d are the source and detector radii, respectively. Overall cylindrical symmetry is assumed. Edwards and McCall [28] have noted the connection between Wolf's result and the spectral power reaching the detector. As long as we have $|u|/v_M < 1-\sigma$ or $|u|/v_M > 1+\sigma$, the ratio of the spectral power incident on the detector to the source spectral radiance is given by the source-detector-symmetric expression:

$$\frac{\Phi_\lambda(\lambda)}{L_\lambda(\lambda)} = D \int_{-1}^{1} \frac{\mathrm{d}x\{(1-x^2)[(2+\sigma x)^2 - \sigma^2]\}^{1/2} L(u, v_\mathrm{M}(1+\sigma x))}{1+\sigma x} \tag{9.62}$$

The leading factor is $D = 4\pi^3 R^4 R_\mathrm{s}^2 R_\mathrm{d}^2 / [d_\mathrm{s}^2 d_\mathrm{d}^2 (\lambda v_\mathrm{M})^2]$, which is source-detector-symmetric and independent of λ. Integration over x can be done using Gauss–Chebyshev quadrature. In a recent calculation that is discussed in the next section, Edwards and McCall have also considered $1 - \sigma < |u|/v_\mathrm{M} < 1 + \sigma$.

9.4.3.2 Case of other optical systems

The preceding SAD problem was relatively self-contained, and the diffraction effects could be quantified in considerable detail. In more complicated optical systems, it may not be possible to break down diffraction effects, in a simple way, into those arising in SAD problems and related analyses without making gross simplifications and incurring significant inaccuracies. However, with care, SAD and related analyses can be used in many—though not all—radiometric situations in multistage optical systems, including one that arose in an actual blackbody calibration [34].

Two examples of the complexities that can arise are illustrated here. Figure 9.8 shows an optical setup that was considered when modeling diffraction effects in an actual blackbody calibration. Diffraction at the edges of the non-limiting apertures Ap 1 and 3 enhanced the irradiance at the detector. The simulated relative excess irradiance at points on the detector is illustrated as a percentage in the bottom panel of Figure 9.9, for the cases of only Ap 3 being present and both apertures being present.

In the top panel, the difference between the two results is shown, both as a dashed curve and as a solid curve based on a combination of the BDW formulation and asymptotic analysis in the spirit of the GTD. The distance of a point on the detector from the optical axis is indicated in the figure by r_d. Near $r_\mathrm{d} = 8.2$ mm, a step is visible in the top panel of Figure 9.9. This can be explained in terms of one of the GTD-type rays bent by Ap 1 being geometrically blocked by the boundary of Ap 3. The model in Reference [34] attempts to address this type of vignetting effect in diffraction calculations and to address some higher-order diffraction effects in terms of SAD and related analyses.

The second example of possible complexities is similar. Figure 9.10 depicts an experimental setup used by Boivin [35] to study diffraction effects of four non-limiting apertures, A_1, A_2, A_3 and A_4, placed in series between a source and detector. The source featured a tungsten lamp that was located behind a 1 mm diameter aperture. In a simulation of the diffraction effects,

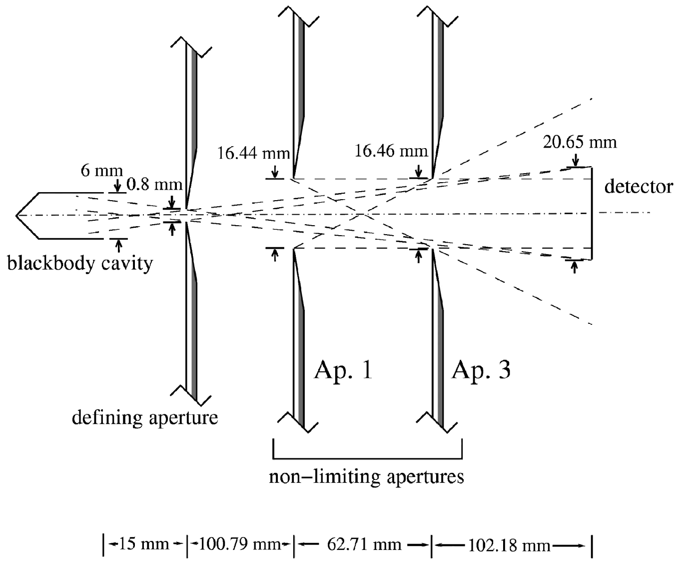

FIG. 9.8. Optical setup used to treat diffraction in a blackbody calibration.

this source was modeled as if the aperture was illuminated by plane waves with angles of incidence not exceeding 0.020 rad from normal. Agreement between measured and simulated diffraction effects indicated that the simulated model of the source was reasonable [26].

The flux reaching the detector for a given plane wave is depicted as a function of the angle of incidence in Figure 9.11. It is normalized so that the total flux incident on the source defining aperture is that aperture's area ($\pi/4$ mm^2). Six results are shown, featuring only A_1, only A_2, only A_3, only A_4, none, or all of the four non-limiting apertures being included in the simulation. The effect of each non-limiting aperture is to deflect excess radiation onto the detector, especially when the perimeter of that aperture is geometrically illuminated through the source defining aperture. Therefore, the effects of a non-limiting aperture can depend on the angle subtended by the simulated lamp filament at the source defining aperture. This subtlety might not be addressed correctly in a casual application of the SAD analysis, but could be treated appropriately using the method found in Reference [34].

9.5 Impacts of Diffraction Effects on Radiometry

We begin with a cursory survey of the radiometry literature dealing with diffraction effects. This survey highlights the insight gained into the role of

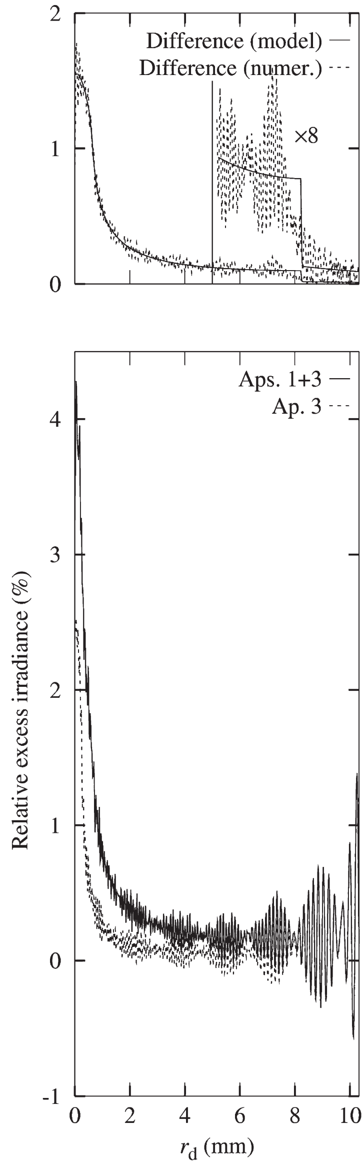

FIG. 9.9. Diffraction-induced irradiance because of non-limiting apertures in Figure 9.8.

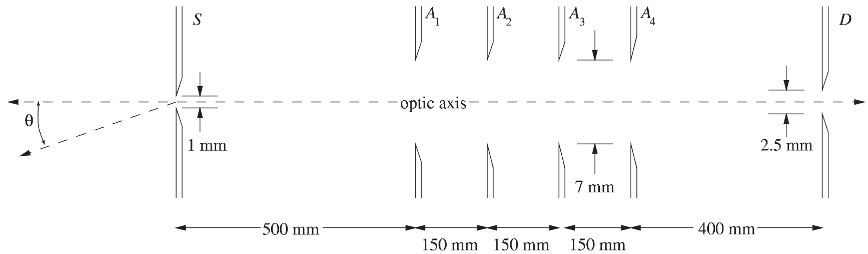

FIG. 9.10. Optical setup featuring four apertures in series studied by Boivin.

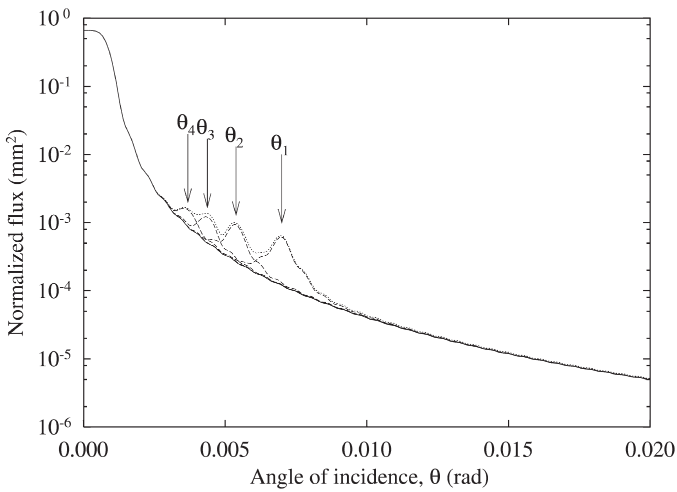

FIG. 9.11. Normalized flux versus plane-wave angle of incidence θ in setup in Figure 9.10. At $\theta = \theta_1$, the perimeter of A_1 is geometrically illuminated, etc.

diffraction effects and the cumulative developments regarding how to estimate or mitigate them. Because this chapter attempts to report the current state of affairs, it should be noted that some of the earlier developments or aspects thereof that are cited in this Section are no longer current.

Much of diffraction theory is formulated for monochromatic radiation, yet radiometric applications frequently involve complex radiation. This mismatch is not fully resolved, but some methods to overcome this mismatch are discussed in Section 9.5.2. These include the *effective-wavelength approximation* and other recent methods for more directly finding total irradiance and power.

Section 9.5.3 mentions three recent examples of diffraction modeling in support of actual radiometric measurements. In order of increasing complexity, these situations involve solar radiometry, spectral calibration of a radiometric telescope, and the already mentioned calibration of a reference blackbody source.

9.5.1 Radiometry Literature Survey

In 1881, Rayleigh [36] derived the fraction of flux in the Airy diffraction pattern enclosed within a circular area in the case of a circular aperture. Rayleigh obtained the well-known result,

$$L(0, v_0) = 1 - J_0^2(v_0) - J_1^2(v_0) \tag{9.63}$$

This was one of the earliest "modern" analyses of diffraction effects in optics. The Airy pattern is a consequence of Fraunhofer diffraction. A strong motivation for analyzing the Airy pattern was its impact on the resolving powers of optics. However, an internally consistent measurement of, say, the spectral irradiance of celestial objects, also requires accounting for diffraction losses, because v_0 depends on wavelength.

The 1885 work by Lommel and 1950s work by Wolf and Focke generalize the Rayleigh result for integrated flux to the case of Fresnel diffraction (or of not being in a focal plane). Some other analyses are included in the volume compiled by Oughstun and cited in the above references. These developments provided a good working model of diffraction effects to study the impact on radiometry. Much of the analysis in the context of radiometry considers the SAD problem, but other topics have also been addressed.

9.5.1.1 Study of the SAD problem

A survey of the radiometric literature shows that a remarkable fraction of the work on diffraction effects was done at or in association with, various national measurement institutes. In 1962, Sanders and Jones [37] discussed the role of diffraction effects and the need to account for them in the context of the then-current "problem of realizing the primary standard of light." Shortly thereafter, Ooba [38] studied the related diffraction effects experimentally.

In 1970, Blevin [39] considered the diffraction loss in the context of the SAD problem for the case of an axial point source, implying $\sigma = 0$, and under-filled detector, implying $|u| < v_M$. (When discussing analysis of the SAD problem, mathematical formulas from the radiometric literature are presented using the SAD notation of this chapter.) Blevin derived a diffraction loss consistent with $L(u, v_M) \cong 1 - 2v_M/[\pi(v_M^2 - u^2)]$, in agreement with earlier work, and confirmed this experimentally for at least two experimental geometries. Blevin used a broadband source and detector, and the diffraction analysis was based on using an *effective-wavelength* *approximation*, an idea that has sometimes been credited to Blevin and is discussed in Section 9.5.3. Note that a more up-to-date evaluation of $L(u, v_M)$ is discussed in Section 9.4.2.

In 1972, Steel et al. [40] provided an approximate extension of Blevin's result to finite σ and analyzed the two cases, $|u| < (1-\sigma)v_M$ and $|u| > (1+\sigma)v_M$. Their results were also extended to allow for the effective-wavelength approximation. Their analysis of the case of a non-limiting aperture ($|u| > (1+\sigma)v_M$) is flawed, as noted by Boivin [41].

Steel et al. also referred to the case of having a limiting aperture as "Case 1" and the case of having a non-limiting aperture as "Case 2." This terminology has become quite standard, so much so that the factor F that describes diffraction effects is often denoted by F_1 or F_2. Recently, Edwards and McCall [28] have also considered the intermediate case of $(1-\sigma)v_M < |u| < (1+\sigma)v_M$, which can be referred to as "Case 3" and which leads to an associated F_3. Edwards and McCall made an insightful geometric construction shown in Figure 9.12 that differentiates the three cases if there is a non-focusing aperture (i.e., $f = \pm\infty$).

In a series of several papers in the 1970s [35, 41–44], Boivin studied diffraction effects along the same lines. Boivin primarily analyzed effects of non-limiting apertures, which are used to reduce stray light. As long as a

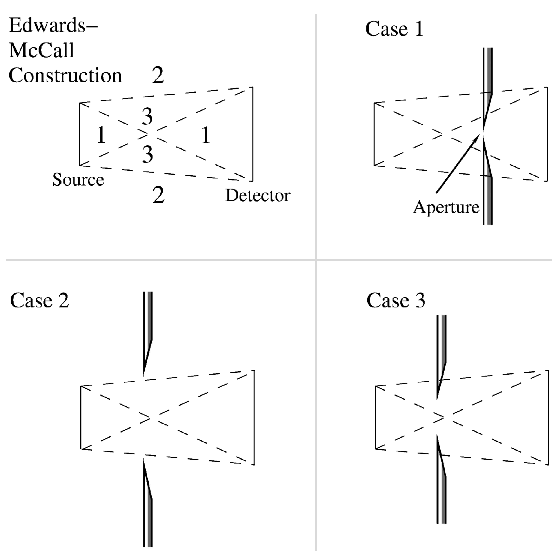

FIG. 9.12. Geometrical construction of Edwards and McCall. Top left: three (disconnected) regions of space are defined by dotted lines. If the rim of an aperture lies within any region, 1, 2, or 3 (as shown), then Cases 1, 2, or 3 applies.

detector is significantly overfilled, Boivin found that a non-limiting aperture gives $F_2(u, v_M) \cong 1 + 2/(\pi v_M)$, both experimentally and theoretically. A more precise result is $F_2(u, v_M) \cong 1 + 2/[\pi v_M(1 - v_M^2/u^2)] + \cdots$, as described in Section 9.4.2. To help establish his reported approximation for F_2, Boivin varied v_s/v_d, the ratio of angles subtended by the source and detector at the center of a non-limiting aperture in an experimental SAD setup. The ratio v_s/v_d was sometimes smaller and sometimes larger than unity.

Boivin recommended that, if possible, a practitioner should use as few apertures as possible in an optical setup, with at most one aperture giving rise to substantial diffraction effects. This is consistent with trying to ensure that the extensive analysis applied to the SAD problem can be almost directly brought to bear in a real optical setup. Boivin also recommended against letting parts of an over-filled detector's area be anywhere near a non-limiting aperture's geometrical shadow boundary. This is at variance with the recent, novel idea of Edwards and McCall, discussed below. (Using the same reasoning by Boivin, a practitioner should also not let an under-filled detector's perimeter be anywhere near the penumbra or fully illuminated region in the case of a limiting aperture.)

Based on an idea attributed to Purcell and Koomen [45], Boivin [35] also experimentally demonstrated that using toothed instead of circular non-limiting apertures can reduce the associated diffraction effects. This was motivated by observing that toothing of an aperture perimeter introduces dephasing and concomitant self-cancellation of U_B at a detector. This idea was subsequently explored and extended theoretically [46], but the author knows of no subsequent applications using toothed non-limiting apertures. It can be difficult to manufacture such apertures, the largest diffraction effects in radiometry are often losses because of limiting apertures, and the effects of non-limiting apertures can often be substantially reduced by modifying the design of an optical setup.

The author has reinvestigated the SAD problem for point and extended sources [47], as well as monochromatic and complex radiation, including radiation from a Planckian source [48]. This has led to more detailed expressions for $F(\lambda)$ and analogous expressions for $\langle F \rangle$ in the case of a Planckian source in the Fraunhofer and Fresnel regimes. A 1998 work introduced the formula found in Eq. (9.62), but the accompanying formulas for $L(u, v_M)$ have been superceded by subsequent work.

Edwards and McCall [28] also recently considered the SAD problem, introducing an algorithm for calculating diffraction effects that is applicable to Case 1–3. These workers consider diffraction effects as a function of intermediate aperture radius for a fixed extended source and detector. Noting that diffraction losses occur for $|u| < (1 - \sigma)v_M$, whereas diffraction gains tend to occur for $|u| > (1 + \sigma)v_M$, Edwards and McCall deduced that diffraction effects on throughput must cross zero at some point when Case 3 applies.

Such a zero crossing can be advantageous and feasible to arrange in some instances in radiometry. A zero crossing should occur nearly simultaneously for a wide range of wavelengths, so that diffraction effects and concomitant uncertainties in measurement results with complex radiation could be greatly reduced. However, a practitioner must also take into account the greater complexity involved in calculating geometrical throughput of the optical setup in Case 3. Furthermore, there are optical setups (for instance, a collimator involving a blackbody cavity, small defining aperture, and collimating mirror to simulate a remote object) for which Case 1 appears unavoidable.

9.5.1.2 Other studies

People have also considered more elaborate optical setups than those that can be mapped onto the SAD problem. In 2001, Suárez-Romero et al. [49] and Shirley and Terraciano [26] independently treated diffraction by a series of optical elements. The former authors made use of the cross-spectral density [50] and analyzed the problem of two apertures in series. The latter authors showed how a practitioner can analyze diffraction in multi-staged cylindrically symmetrical systems using Gaussian-optics and full Kirchhoff and Rayleigh–Sommerfeld treatments, with an arbitrary number of apertures in series. Two examples of the application of the latter development were already mentioned in Section 9.4.3.2, and two additional examples are mentioned in Sections 9.5.3.1 and 9.5.3.2.

Much less work regarding diffraction effects in radiometry has been done for cases without cylindrical symmetry. It is well known that the multiple integrations in Eq. (9.29), which does not assume cylindrical symmetry, can be done one aperture at a time by use of fast Fourier-transform (FFT) techniques [51]. Care must be taken during such a procedure to appropriately account for curved perimeters of optical surfaces, in order to faithfully reproduce the part of a wave front corresponding to U_{B}. In the case of cylindrical symmetry, the double loops over radial coordinates r and s implicit in Eq. (9.25) of Reference [26] can also be accelerated by FFT methods. This can be realized by using logarithmic radial meshes that are spaced at regular intervals of the logarithm of r or s within a Gaussian-optics analysis.

9.5.2 Complex Radiation

Virtually all of the analysis presented thus far in this chapter has involved monochromatic radiation, but many radiometric applications involve complex radiation. In the diffraction analysis for complex radiation, the effective-wavelength approximation has been of longstanding use, and methods recently developed for directly evaluating diffraction effects on total irradiance and total power have also been recently introduced [48, 52].

9.5.2.1 Effective-wavelength approximation

Formulas for diffraction effects in Section 9.4 and the lowest-order expressions cited above indicate that $\varepsilon_{\mathrm{diff}}(\lambda)$ can scale approximately linearly with λ. Assuming exact proportionality, Blevin noted that Eq. (9.4) becomes

$$\langle F \rangle = F(\lambda_{\mathrm{e}}) \tag{9.64}$$

with the *effective wavelength* λ_{e} being

$$\lambda_{\mathrm{e}} = \frac{\int_0^\infty \mathrm{d}\lambda \lambda R(\lambda) M(\lambda) L_\lambda(\lambda)}{\int_0^\infty \mathrm{d}\lambda R(\lambda) M(\lambda) L_\lambda(\lambda)} \tag{9.65}$$

Note that the product $R(\lambda)M(\lambda)$ can include a factor that realizes effects of the spectral luminous efficiency function $V(\lambda)$. Hence, as shown by Blevin, the effective-wavelength approximation can be used in subfields of radiometry other than absolute radiometry, such as photometry. Because $F(\lambda)$ contains oscillatory terms that tend to average to nearly zero upon integration over wavelength, better approximations to Eq. (9.4) are often obtained in the effective-wavelength approximation if $F(\lambda_{\mathrm{e}})$ is computed with oscillatory terms omitted. Otherwise, their inclusion at a discrete wavelength (λ_{e}) is not representative of the result found after averaging over a spectrum.

9.5.2.2 Diffraction effects on total irradiance

If we introduce

$$\begin{aligned} f(l) = &\iint_{Ap1} \mathrm{d}x_1 \mathrm{d}y_1 \ldots \iint_{ApN} \mathrm{d}x_N \mathrm{d}y_N \\ &\times \delta\left(d_0 + d_1 + \cdots + d_N + \sum_{\mu,\nu=0}^{N+1} B_{\mu\nu}(x_\mu x_\nu + y_\mu y_\nu) - l \right) \end{aligned} \tag{9.66}$$

Eq. (9.29) can be rewritten as

$$U(\mathbf{x}_{\mathrm{d}}) \cong \frac{U_0}{(\mathrm{i}\lambda)^N d_0 d_1 \ldots d_N} \int_{-\infty}^{+\infty} \mathrm{d}l \mathrm{e}^{\mathrm{i}ql} f(l) \tag{9.67}$$

Rearranging and squaring Eq. (9.67) gives

$$X(\lambda; \mathbf{x}_\mathrm{d}, \mathbf{x}_\mathrm{s}) = \left|\frac{U(\mathbf{x}_\mathrm{d})}{U_0}\right|^2 \cong (\lambda^N d_0 d_1 \ldots d_N)^{-2} \int_{-\infty}^{+\infty} \mathrm{d}l \int_{-\infty}^{+\infty} \mathrm{d}l' \mathrm{e}^{\mathrm{i}q(l-l')} f(l) f(l') \tag{9.68}$$

Here $X(\lambda; \mathbf{x}_\mathrm{d}, \mathbf{x}_\mathrm{s})$ is a type of transfer function.

The detector-responsivity-weighted irradiance at $\mathbf{x}_\mathrm{d}$,

$$E'(\mathbf{x}_\mathrm{d}) = \int_0^\infty \mathrm{d}\lambda\, R(\lambda) E_\lambda(\lambda; \mathbf{x}_\mathrm{d}) \tag{9.69}$$

may be considered as arising from the sum of contributions from area elements of the source, according to

$$E'(\mathbf{x}_\mathrm{d}) = \int_{A_\mathrm{s}} \mathrm{d}^2\mathbf{x}_\mathrm{s} \int_0^\infty \mathrm{d}\lambda\, R(\lambda) X(\lambda; \mathbf{x}_\mathrm{d}, \mathbf{x}_\mathrm{s}) L_\lambda(\lambda; \mathbf{x}_\mathrm{s}) \tag{9.70}$$

We may substitute the definition of $X(\lambda; \mathbf{x}_\mathrm{s}, \mathbf{x}_\mathrm{s})$ given in Eq. (9.68) into the integral Eq. (9.70). If we change the variable of integration over the spectrum from λ to q, using $q = 2\pi/\lambda$ and $\mathrm{d}\lambda = -2\pi\, \mathrm{d}q/q^2$, after a little rearrangement we obtain

$$E'(\mathbf{x}_\mathrm{d}) = \frac{(2\pi)^{1-2N}}{(d_0 d_1 \ldots d_N)^2} \int_{A_\mathrm{s}} \mathrm{d}^2\mathbf{x}_\mathrm{s} \int_{-\infty}^{+\infty} \mathrm{d}l \int_{-\infty}^{+\infty} \mathrm{d}l' f(l) f(l') \int_0^\infty \mathrm{d}q \\ \times q^{2N-2} R(\lambda) L_\lambda(\lambda; \mathbf{x}_\mathrm{s}) \mathrm{e}^{\mathrm{i}q(l-l')} \tag{9.71}$$

Dependence of $f(l)$ and $f(l')$ on $\mathbf{x}_\mathrm{s}$ is implicit.

If $L_\lambda(\lambda; \mathbf{x}_\mathrm{s})$ is separable regarding its spectral and spatial dependences, according to $L_\lambda(\lambda; \mathbf{x}_\mathrm{s}) = a(\lambda) b(\mathbf{x}_\mathrm{s})$, the integration in Eq. (9.71) is analogously separable. In this case, evaluation of Eq. (9.71) is greatly simplified. For a Planckian source with emissivity ε, giving

$$L_\lambda(\lambda; \mathbf{x}_\mathrm{s}) = \frac{\varepsilon c_1}{\pi \lambda^5} \left[\exp\left(\frac{c_2}{\lambda T}\right) - 1\right]^{-1} \tag{9.72}$$

and a spectrally flat detector with $R(\lambda) = R_0$, we have

$$\begin{aligned} E'(\mathbf{x}_\mathrm{d}) &= \frac{(2\pi)^{-4-2N} \varepsilon c_1 R_0}{\pi (d_0 d_1 \ldots d_N)^2} \int_{A_\mathrm{s}} \mathrm{d}A_\mathrm{s} \int_{-\infty}^{+\infty} \mathrm{d}l \int_{-\infty}^{+\infty} \mathrm{d}l' f(l) f(l') \int_0^\infty \frac{\mathrm{d}q q^{2N+3} \mathrm{e}^{\mathrm{i}q(l-l')}}{\mathrm{e}^{\beta q} - 1} \\ &= \frac{(2\pi)^{-5-2N} (2N+3)! \varepsilon c_1 R_0}{(d_0 d_1 \ldots d_N)^2} \int_{A_\mathrm{s}} \mathrm{d}A_\mathrm{s} \int_{-\infty}^{+\infty} \mathrm{d}l \\ &\quad \times \int_{-\infty}^{+\infty} \mathrm{d}l' f(l) f(l') S_{2N+4}(\beta, l - l') \end{aligned} \tag{9.73}$$

with $\beta = c_2/(2\pi T)$ and $S_\nu(x, y) = \sum_{n=1}^{\infty} [(nx + \mathrm{i}y)^{-\nu} + (nx - \mathrm{i}y)^{-\nu}]$.

The remaining integrals have smoother integrands, permitting coarser numerical sampling, than their monochromatic counterparts, which have intrinsically oscillatory integrands. The utility of Eq. (9.73) has been demonstrated in Reference [52], which also shows how $S_4(x, y)$ in the present notation can be efficiently evaluated. It is also in principle possible to generalize Eq. (9.73) to optical setups with other forms of $R(\lambda)L_\lambda(\lambda; \mathbf{x}_\mathrm{s})$ while continuing to exploit separability of $L_\lambda(\lambda; \mathbf{x}_\mathrm{s})$.

Expressions for integrated total flux in the case of a Planckian source have also been derived. These are analogous to Wolf's expressions for integrated spectral flux. As an important example, in the case of Fraunhofer diffraction by a limiting circular aperture, the fraction of total power incident on the aperture that reaches a circular detector is [48]

$$F(\sigma) = 1 - \frac{4\zeta(3)A}{6\pi\zeta(4)} + \frac{A^3 \log_\mathrm{e} A}{24\pi\zeta(4)} + \frac{(3 - 2\gamma - 6\log_\mathrm{e} 2)A^3}{48\pi\zeta(4)} + O(A^5 \log_\mathrm{e} A) \quad (9.74)$$

with $A = c_2/[(1 + \sigma)v_\mathrm{M}\lambda T]$, $\zeta(z)$ being the Riemann zeta function, and $\gamma \cong 0.577216$ the Euler's constant. The parameter A depends on σ, T, and the geometry. However, A does not depend on v_M or λ separately, because we have $v_\mathrm{M} \propto \lambda^{-1}$, so that the product λv_M is a wavelength-independent, geometrical entity. In the spirit of Eq. (9.62), this gives

$$\frac{\Phi}{L} = D \int_{-1}^{1} \frac{\mathrm{d}x\{(1 - x^2)[(2 + \sigma x)^2 - \sigma^2]\}^{1/2} F(\sigma x)}{1 + \sigma x} \quad (9.75)$$

which relates total power to total source radiance including diffraction effects.

9.5.3 Practical Examples

Three practical examples of diffraction effects in radiometry are presented below. These are solar radiometry, blackbody calibration of a telescope used to measure spectral irradiance of celestial objects, and calibration of a standard reference blackbody.

9.5.3.1 Solar radiometry

The layouts of two different absolute solar radiometers are shown in Figure 9.13. The PMO6 radiometer [53] features a view-limiting aperture that acts as a non-limiting aperture between the extended source (sun) and the defining aperture placed in front of an absolute radiometer. The SAD geometry is defined by $R = 4.25$ mm, $R_\mathrm{d} = 2.5$ mm, $d' = 95.4$ mm, $d \cong 1.5 \times 10^{14}$ mm, and $R_\mathrm{s} \cong 6.75 \times 10^{11}$ mm. If we model the sun as a 5900 K Planckian source, the corresponding version of Eq. (9.75) for the Fresnel regime and a non-limiting aperture gives $\langle \varepsilon_\mathrm{diff} \rangle \cong 0.0012798$,

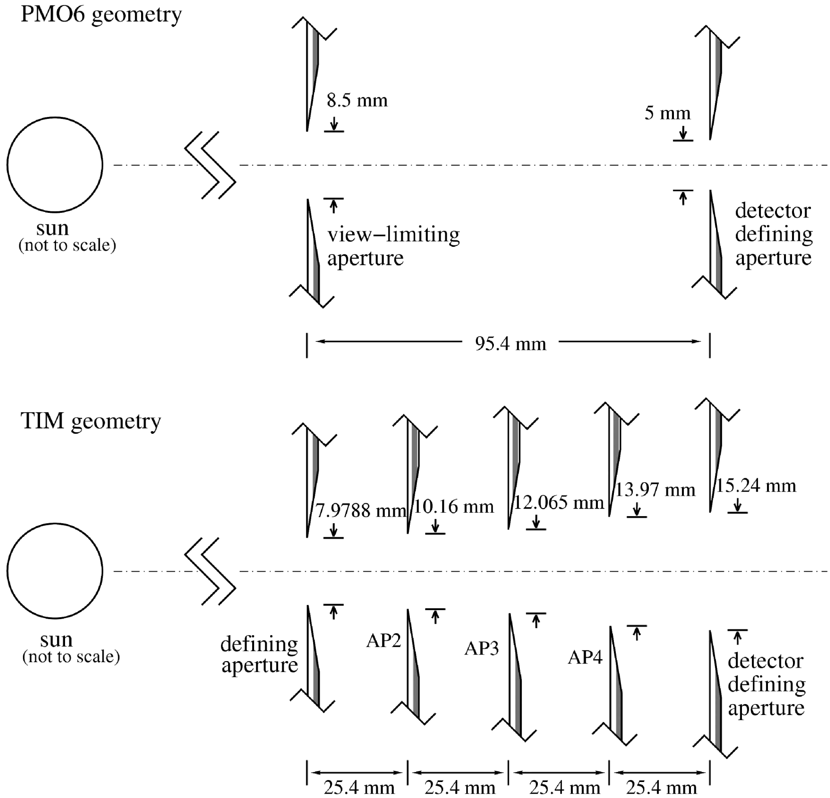

FIG. 9.13. Layouts of two solar radiometers.

implying that about 0.13% excess power reaches the detector compared to that expected from the geometrical throughput. This result automatically includes integration with respect to wavelength over the entire spectrum. In comparison, the effective-wavelength approximation gives $\langle \varepsilon_{\mathrm{diff}} \rangle \cong 0.0012720$ if oscillatory terms are neglected and $\langle \varepsilon_{\mathrm{diff}} \rangle \cong 0.0011656$ if oscillatory terms are (unadvisedly) included.

The total-irradiance monitor (TIM) instrument [54], which is also used in absolute solar radiometry, features a $R = 3.9894$ mm defining aperture that is $d' = 101.6$ mm from a $R_{\mathrm{d}} = 7.62$ mm radiometer entrance. Three intervening, non-limiting apertures (labeled AP2, AP3, and AP4) are also noted. These non-limiting apertures are barely large enough to permit passage of all marginal rays from the perimeter of the defining aperture to the perimeter of the radiometer entrance. This makes it difficult to treat their diffraction effects using asymptotic methods. If the non-limiting apertures are ignored, the SAD problem leads to a diffraction loss of total power given by $\langle \varepsilon_{\text{diff}} \rangle \cong -0.000432$. If the non-limiting apertures are taken into account, this loss is barely unchanged, based on calculations using the method of Reference [26].

9.5.3.2 Calibration of a radiometric telescope

Figure 9.14 shows an unfolded, model optical setup used to simulate diffraction effects in a blackbody calibration of a radiometric telescope [55]. A calibrated blackbody with a 10 mm radius diameter cavity opening (I) is 100 mm behind a $R_s = 1.778$ mm radius aperture (II), which is 150 mm from a $R_d = 6.35$ mm radius detector (IV). To help simulate a remote object, a pinhole aperture (III) with diameter $2R = 202$ μm or $2R = 262$ μm is located 23 mm downstream from the 1.778 mm aperture and 127 mm upstream from the detector. In the real optical setup, a fold mirror was located at the position corresponding to the model's detector, and a focusing mirror had one focus on the pinhole aperture and concentrated radiation onto a spectrometer entrance. In a field deployment, the telescope optics would have one focus at infinity and concentrate radiation onto the same spectrometer entrance in similar fashion.

If we treat the last three optical elements (II–IV) as a SAD setup, the diffraction effects indicated by the solid curves in Figure 9.15 are obtained. If instead the 100 mm separation between I and II is taken into account, and the system is treated according to Reference [26], the diffraction effects indicated by the dashed curves in Figure 9.15 are obtained. This further illustrates both the significance of diffraction effects in a measurement and the potential need to go beyond the SAD model.

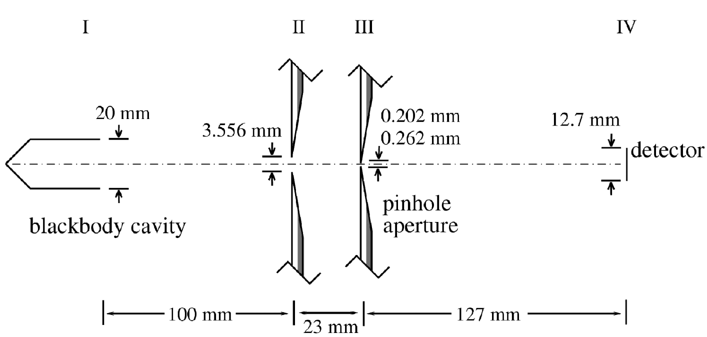

FIG. 9.14. Setup used to calibrate a radiometric telescope.

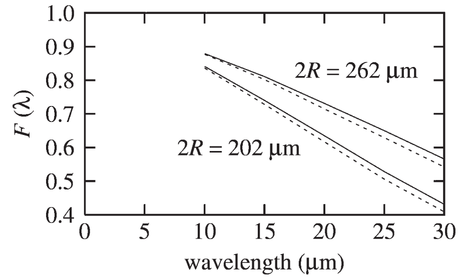

FIG. 9.15. Diffraction effects on spectral throughput of setup shown in Figure 9.14. The solid lines indicate a SAD treatment, whereas the dashed lines indicate a more complete treatment.

9.5.3.3 Blackbody calibration

Diffraction effects that arose in an actual blackbody calibration were already discussed in Section 9.4.3.2 and in Reference [34]. These included significant losses at the defining aperture, partially compensating gains because of non-limiting apertures, and the need to go beyond the SAD model as discussed further in Reference [34]. Other blackbody calibrations have repeatedly raised similar issues.

9.5.4 Diffraction Effects and Measurement Uncertainties

To illustrate the role of diffraction effects in measurement uncertainties, note that Eq. (9.3) gives

$$U_{\mathrm{R}}^2(T(\lambda)) = U_{\mathrm{R}}^2(F(\lambda)) + U_{\mathrm{R}}^2(T_0) + U_{\mathrm{R}}^2(M(\lambda)) + \cdots \tag{9.76}$$

Here $U_{\mathrm{R}}(X)$ denotes the relative uncertainty of the quantity X, and terms involving correlations of the factors $F(\lambda)$, T_0 and $M(\lambda)$ are not explicitly noted.

Note that, for numerical reasons and for systematic reasons related to use of an approximate theory, the correct value of $F(\lambda)$ is not precisely known, and its uncertainty contributes to the overall uncertainty of a measurement. Obviously, ignoring diffraction effects does not reduce overall measurement uncertainties. Rather, theoretical and/or experimental diffraction analysis can reduce and better define the actual uncertainties by better determining the value of $F(\lambda)$.

It has been difficult to determine the uncertainty of the theoretical $F(\lambda)$, in part because measurements of $F(\lambda)$ intended to compare theory and the "correct" result have appreciable uncertainties. All indications are that the

Kirchhoff theory can be accurate to within a few percent of $\varepsilon_{\mathrm{diff}}(\lambda)$, say about 5%. However, this estimate remains to be confirmed.

Statistical correlations that are suppressed in Eq. (9.76) can also be important, and it is desirable to ensure that correlations and other systematic effects are kept as similar as possible between characterization of optical instrumentation and its application. In this way, diffraction effects, statistical correlations in the measurement equation and other aspects of performance can be experimentally and/or theoretically determined and compensated. The transmittance of such information is an indispensable part of reports on measurements. To accomplish this, Wyatt et al. note [1]: "A cardinal rule of calibration is that one should calibrate…under the same conditions [as usage]."

9.6 Radiometry of Novel Sources

Thus far, the discussion in this chapter has been phrased in terms of tracing the energy flow from points $\{\mathbf{r}_\mathrm{s}\}$ on a "source" surface to points $\{\mathbf{r}_\mathrm{d}\}$ on a "detector" surface. Between the source and detector, the wave nature of the radiation was respected and approximately described using the Kirchhoff theory. By summing irradiance at the detector over source points $\{\mathbf{r}_\mathrm{s}\}$, mutual incoherence of waves originating at different points was implicitly assumed.

Walther [56] called attention to this and related issues in 1968. To help generalize the classical, local definition of radiance, Walther introduced a "generalized radiance function." For radiation emitted from around a point $\mathbf{r}_\mathrm{s}$ into the direction $\hat{\mathbf{s}}$, Walther's function can be given by

$$B(\mathbf{r}_\mathrm{s}, \hat{\mathbf{s}}, \omega) = \frac{\cos\theta}{\lambda^2}\int \mathrm{d}^2\mathbf{r}'\, W^{(0)}(\mathbf{r}_\mathrm{s} + \mathbf{r}'/2, \mathbf{r}_\mathrm{s} - \mathbf{r}'/2, \omega)\exp(-\mathrm{i}k\hat{\mathbf{s}}\cdot\mathbf{r}') \qquad (9.77)$$

where

$$W^{(0)}(\mathbf{x}, \mathbf{x}', \omega) = \int_{-\infty}^{+\infty} \mathrm{d}\tau \exp(+\mathrm{i}\omega\tau)\langle V(\mathbf{x}, t)V^*(\mathbf{x}', t+\tau)\rangle \qquad (9.78)$$

is the cross-spectral density for two points $\mathbf{x}$ and $\mathbf{x}'$ at frequency ω, angle brackets indicate temporal averaging, and V denotes a radiation field amplitude function in the same spirit as does U. There are pathologies associated with Walther's generalized radiance function, as discussed by others [57]. However, it does help to bridge the gap between real sources and the traditional, "local" definition of radiance used in classical radiometry.

An important result of further analysis made possible by Eqs. (9.77) and (9.78) is that traditional radiometric concepts such as radiance require no substantial modification for many incoherent sources, including blackbodies. This is discussed by Nugent and Gardner [58], Gardner [59], and Mielenz [60], whose work was stimulated in part by issues raised by Wolf [61].

Currently, there is also interest in using a synchrotron as a standard radiation source [62]. The spectral and spatial characteristics of synchrotron radiation can be computed if the electron energy, electron beam current and geometrical parameters of the electrons' orbit are known (see [4], pp. 672–679). In this case, the radiation in a plane near an electron is certainly not incoherent, and the concept of a generalized radiance function must be reconsidered. However, once the radiation field is known, for instance, at the first aperture through which the radiation passes, the Kirchhoff theory should still be useful for understanding subsequent propagation of this and other novel forms of radiation.

References

1. C. L. Wyatt, V. Privalsky, and R. Datla, in "Recommended Practice; Symbols, Terms, Units and Uncertainty Analysis for Radiometric Sensor Calibration. NIST Handbook 152." U.S. Govt. Printing Office, Washington, DC, USA, 1998.
2. W. T. Welford, "Geometrical Optics." North-Holland Publishing Company, Amsterdam, 1962.
3. A. Walther, "The Ray and Wave Theory of Lenses." Cambridge University Press, Cambridge, UK, 1995.
4. J. D. Jackson, "Classical Electrodynamics," 2nd edition. Wiley, New York, USA, 1975.
5. S. G. Johnson and J. D. Joannopoulos, "Photonic Crystals: The Road from Theory to Practice." Kluwer Academic Publishers, Boston, USA, 2002.
6. G. Kirchhoff, Zur Theorie der Lichtstrahlen, *Ann. Physik* 254, 663–695 (1883).
7. M. Born and E. Wolf, "Principles of Optics." Pergamon Press Ltd., Oxford, UK, 1965.
8. A. Sommerfeld, "Optics." Academic Press, New York, USA, 1954.
9. A. Sommerfeld, Mathematische theorie der diffraction, *Math. Ann.* 47, 317–374 (1896).
10. H. A. Bethe, Theory of diffraction by small holes, *Phys. Rev.* 66, 163–182 (1944).
11. C. J. Bouwkamp, On Bethe's theory of diffraction by small holes, *Philips Res. Rep.* 5, 321–332 (1950).

12. H. Levine and J. Schwinger, On the theory of diffraction by an aperture in an infinite plane screen I, *Phys. Rev.* 74, 958–974 (1948); On the theory of diffraction by an aperture in an infinite plane screen II, *Phys. Rev.* 75, 1423–1432 (1949).
13. W. Braunbek, Neue Näherungsmethode für die Beugung am ebenen Schirm, *Z. Phys.* 127, 381–390, 1950); Zur Beugung an der Kreisscheibe, *Z. Phys.* 127, 405–415 (1950); Zur Beugung an der kreisförmigen Öffnung, *Z. Phys.* 138, 80–88 (1954).
14. K. D. Mielenz, Optical diffraction in close proximity to plane apertures. I. Boundary-value solutions for circular apertures and slits, *J. Res. Natl. Inst. Stand. Technol.* 107, 355–362 (2002); Optical diffraction in close proximity to plane apertures. II. Comparison of half-plane diffraction theories, *J. Res. Natl. Inst. Stand. Technol.* 108, 57–68 (2003); Optical diffraction in close proximity to plane apertures. III. Modified, self-consistent theory, *J. Res. Natl. Inst. Stand. Technol.* 109, 457–464 (2004).
15. K. E. Oughstun, "Selected Papers on Scalar Wave Diffraction." SPIE Optical Engineering Press, Bellingham, USA, 1992.
16. G. A. Maggi, *Ann. Mat.* IIa(16), 21ff (1888).
17. A. Rubinowicz, Die Beugungswelle in der Kirchhoffschen Theorie der Beugungserscheinungen, *Ann. Physik.* 53, 257–278 (1917).
18. K. Miyamoto, E. Wolf, Generalization of the Maggi–Rubinowicz theory of the boundary diffraction wave—Part I, *J. Opt. Soc. Am.* 52, 615–625 (1962); Generalization of the Maggi–Rubinowicz theory of the boundary diffraction wave—Part II, *J. Opt. Soc. Am.* 52, 626–637 (1962).
19. E. Wolf and E. Marchand, Comparison of the Kirchhoff and the Rayleigh–Sommerfeld theories of diffraction at an aperture, *J. Opt. Soc. Am.* 54, 587–594 (1964).
20. J. B. Keller, Geometrical theory of diffraction, *J. Opt. Soc. Am.* 52, 116–130 (1962).
21. G. L. James, "Geometrical Theory of Diffraction." Peter Peregrinus Ltd., London, UK, 1986.
22. V. A. Borovikov and B. Ye. Kinber, "Geometrical Theory of Diffraction." Inst. Elect. Engineers, London, UK, 1994.
23. R. K. Luneburg, "Mathematical Theory of Optics." Cambridge University Press, London, UK, 1966.
24. E. Lommel, Die Beugungserscheinungen einer kreisrunden Oeffnung und eines kreisrunden Schirmschens theoretisch und experimentell Bearbeitet, *Abh. Bayer. Akad.* 15, 233–328 (1885).
25. K. D. Mielenz, Algorithms for Fresnel diffraction at rectangular and circular apertures, *J. Res. Natl. Inst. Stand. Technol.* 103, 497–509 (1998).

26. E. L. Shirley and M. L. Terraciano, Two innovations in diffraction calculations for cylindrically symmetrical systems, *Appl. Opt.* 40, 4463–4472 (2001).
27. E. L. Shirley and E. K. Chang, Accurate efficient evaluation of Lommel functions for arbitrarily large arguments, *Metrologia* 40, S5–S8 (2003).
28. P. Edwards and M. McCall, Diffraction loss in radiometry, *Appl. Opt.* 42, 5024–5032 (2003).
29. E. Wolf, Light distribution near focus in an error-free diffraction image, *Proc. Roy. Soc. A* 204, 533–548 (1951).
30. J. Focke, Total illumination in an aberration-free diffraction image, *Optica Acta* 3, 161–163 (1956).
31. K. Schwarzschild, *Sitz. Ber. Bayer. Akad. Wiss.* 28, 271 (1898).
32. N. G. van Kampen, An asymptotic treatment of diffraction problems, *Physica* 14, 575–589 (1949).
33. F. W. J. Olver, "Asymptotics and special functions." A.K. Peters, Ltd., Wellesley, USA, 1997.
34. E. L. Shirley, Intuitive diffraction model for multistaged optical systems, *Appl. Opt.* 43, 735–743 (2004).
35. L. P. Boivin, Reduction of diffraction errors in radiometry by means of toothed apertures, *Appl. Opt.* 17, 3323–3328 (1978).
36. Lord Rayleigh, On images formed without reflection or refraction, *Phil. Mag.* 11, 214–218 (1881).
37. C. L. Sanders and O. C. Jones, Problem of realizing the primary standard of light, *J. Opt. Soc. Am.* 52, 731–742 (1962).
38. N. Ooba, Experimental study on diffraction in the measurement of the primary standard of light, *J. Opt. Soc. Am.* 54, 357–361 (1964).
39. W. R. Blevin, Diffraction losses in radiometry and photometry, *Metrologia* 6, 39–44 (1970).
40. W. H. Steel, M. De, and J. A. Bell, Diffraction corrections in radiometry, *J. Opt. Soc. Am.* 62, 1099–1103 (1972).
41. L. P. Boivin, Diffraction corrections in radiometry: Comparison of two different methods of calculation, *Appl. Opt.* 14, 2002–2009 (1975).
42. L. P. Boivin, Diffraction losses associated with Tungsten lamps in absolute radiometry, *Appl. Opt.* 14, 197–200 (1975).
43. L. P. Boivin, Diffraction corrections in the radiometry of extended sources, *Appl. Opt.* 15, 1204–1209 (1976).
44. L. P. Boivin, Radiometric errors caused by diffraction from circular apertures: Edge effects, *Appl. Opt.* 16, 377–384 (1977).
45. J. D. Purcell and M. J. Koomen, "Coronagraph with Improved Scattered-Light Properties. Report of NRL Progress." Govt. Printing Office, Washington, DC, USA, 1962.

46. E. L. Shirley and R. U. Datla, Optimally toothed apertures for reduced diffraction, *J. Res. Natl. Inst. Stand. Technol.* 101, 745–753 (1996).

47. E. L. Shirley, Revised formulas for diffraction effects with point and extended sources, *Appl. Opt.* 37, 6581–6590 (1998).

48. E. L. Shirley, Fraunhofer diffraction effects on total power for a Planckian source, *J. Res. Natl. Inst. Stand. Technol.* 106, 775–779 (2001); Diffraction corrections in radiometry: Spectral and total power, and asymptotic properties, *J. Opt. Soc. Am. A* 21, 1895–1906 (2004).

49. J. G. Suárez-Romero, E. Tepíchin-Rodríguez, and K. D. Mielenz, Cross-spectral density propagated through a circular aperture, *Metrologia* 38, 379–384 (2001).

50. L. Mandel and E. Wolf, "Optical Coherence and Quantum Optics." Cambridge University Press, Cambridge, UK, 1975.

51. J. W. Goodman, "Introduction to Fourier Optics," 2nd edition. McGraw-Hill, New York, USA, 1996.

52. E. L. Shirley, Diffraction effects on broadband radiation: Formulation for computing total irradiance, *Appl. Opt.* 43, 2609–2620 (2004).

53. R. W. Brusa and C. Fröhlich, Absolute radiometers (PMO6) and their experimental characterization, *Appl. Opt.* 25, 4173–4180 (1986).

54. G. M. Lawrence, G. Kopp, G. Rottman, J. Harder, T. Woods, and H. Loui, Calibration of the total irradiance monitor, *Metrologia* 40, S78–S80 (2003).

55. F. C. Witteborn, M. Cohen, J. D. Bregman, D. H. Wooden, K. Heere, and E. L. Shirley, Spectral irradiance calibration in the infrared. XI. Comparison of α Bootis and 1 Ceres with a laboratory standard, *Astron. J.* 117, 2552–2560 (1999).

56. A. Walther, Radiometry and coherence, *J. Opt. Soc. Am.* 58, 1256–1259 (1968).

57. E. Wolf, Coherence and radiometry, *J. Opt. Soc. Am.* 68, 6–17 (1978).

58. K. A. Nugent and J. L. Gardner, Radiometric measurements and correlation-induced spectral changes, *Metrologia* 29, 319–324 (1992).

59. J. L. Gardner, Partial coherence and practical radiometry, *Metrologia* 30, 419–423 (1993).

60. K. D. Mielenz, "Wolf shifts" and their physical interpretation under laboratory conditions, *J. Res. Natl. Inst. Stand. Technol.* 98, 231–240 (1993).

61. E. Wolf, Invariance of the spectrum of light on propagation, *Phys. Rev. Lett.* 56, 1370–1372 (1986).

62. G. Ulm, Radiometry with synchrotron radiation, *Metrologia* 40, S101–S106 (2003); P.-S. Shaw, U. Arp, H. W. Yoon, R. D. Saunders, A. C. Parr, and K. R. Lykke, A SURF beamline for synchrotron source-based absolute radiometry, *Metrologia* 40, S124–S127 (2003).